学位論文

A Gustatory Neural Circuit of *Caenorhabditis elegans* Generates Memory-Dependent Behaviors in Na^+ Chemotaxis

(線虫 ***Caenorhabditis elegans***
のナトリウムイオンに対する記憶依存の
化学走性を制御する神経回路の解明)

平成 28 年 7 月博士(理学)申請

東京大学大学院理学系研究科
生物化学専攻

王 丽芳

Abstract

Animals generate various behaviors in response to environmental chemicals, which are often plastic depending on previous experiences. This behavioral plasticity is important for survival in various environments. *Caenorhabditis elegans* has a highly developed chemosensory system, although it senses chemicals using a limited number of sensory neurons. Besides, it also possesses many genes homologous to those expressed in vertebrate brains, which makes it an ideal model for analyzing the functions of neurons in innate and learned behaviors. In this study, I describe a new type of memory-dependent behavioral plasticity in *C. elegans*: a plasticity in Na^+ chemotaxis generated by a gustatory neuron ASEL (ASE-left). When worms were cultivated in the presence of Na^+, they showed positive chemotaxis to Na^+; but when worms were cultivated under Na^+-free conditions, they showed no Na^+ concentration preference. Optogenetics combined with behavioral quantification with worm tracking system recapitulated the chemotaxis responses: worms showed reduction of the reversal/turning frequency upon activation of ASEL when they were pre-cultured in Na^+-present conditions; whereas, worms showed no response when they were transferred from Na^+-free cultivation conditions to Na^+-present conditions. Besides, ChR2-driven stimulation of ASEL evoked an increase in intracellular Ca^{2+} only after cultivation with Na^+. Under the conditions of cultivation with Na^+, the first layer downstream interneurons AIB, AIY, and AIA, which have synapses with ASEL, were all found to be involved in regulating the behavioral responses generated by ASEL. Photostimulation of ASEL activated downstream interneurons AIY and AIA to promote forward locomotion, while it inhibited AIB to prevent the reversal/turning behavior, which overall drive worms towards higher concentrations. I also found that the Gq signaling pathway and the glutamatergic neurotransmission are involved in the behavioral response generated by ASEL.

Table of content

1. Introduction

1.1 Research on behavioral plasticity in learning and memory

The capabilities of learning and memory are widespread in the animal kingdom including human. By virtue of this ability, animals can search for places where plenty of tasted food and water exist, and move to the environment with appropriate temperature and moisture according to previous experience. The mechanism of learning and memory, namely, sensing environmental stimuli, storing memory, and executing learned behaviors, has been a major unanswered question for scientists for years. However, there have been difficulties in the study using human and mammals as research samples, because of their complicated nervous system and the ethical limits. Nevertheless, learning and memory, as basic capabilities for survival, are conserved among organisms during the long evolution. Therefore invertebrates have played an important role in understanding how the neural circuits generate adaptive behavioral changes by learning and memory because of their simple neural circuits and greater experimental accessibility. Kandel and colleagues began behavioral plasticity research using the marine mollusc *Aplysia* in 1960s (Kandel and Tauc, 1965), and revealed that memory-generated behavioral changes are caused by synaptic plasticity (Kandel. 2001). In 1970s, Sydney Brenner (1974) began his research on the development and neural functions of *Caenorhabditis elegans*, which is currently well-known model organism. Cell biology and molecular genetics of *C. elegans* broadens knowledge on behavioral plasticity (Bargmann, 2006; Ardiel and Rankin, 2010; Sasakura and Mori, 2012). In 1980s, Farley and Alkon (1985) revealed the essential cellular mechanism of associative learning in *Hermissenda*. The behavioral molecular genetics of *Drosophila* improves our knowledge on the nervous system enormously (Waddell and Quinn, 2001). Invertebrate studies have showed that biological basis of learning is highly conserved (Burne et al., 2011; Glanzman, 2010; Stein and Murphy, 2014).

1.2 *C. elegans* as an ideal model for chemotaxis

C. elegans is one of the most extensively studied organism in biological research because of the following characteristics: 1) small (~1mm) and transparent body which makes observation and manipulation easy using microscope; 2) short life cycle (<4d) and ease of laboratory cultivation are beneficial for developmental research; 3) self-fertilizing hermaphrodites can easily generate inbred lines, and they can also reproduce by mating with males for introducing different genetic architecture; 4) only 959 somatic cells make up the adult hermaphrodite body.

Fig. Intro1. Diagrams of an adult hermaphrodite.
a, Differential interference contrast (DIC) image of an adult hermaphrodite, Scale bar 0.1 mm. ***b***, A schematic of anatomical structures. (Adapted from wormatlas: http://www.wormatlas.org/hermaphrodite/introduction/Introframeset.html)

Whites et al. (1986) described a wiring diagram of the nervous system of *C. elegans* by reconstructing a serial section of electron microscope images, which consist of the 302 neurons, 5000 chemical synapses, 600 gap junctions, and 2000 neuromuscular junctions in the case of adult hemaphrodite (Fig. Intro2). Furthermore, *C. elegans* genome carries many genes homologous to those expressed in vertebrate brains. *C. elegans* has a highly developed chemosensory system. Sixteen pairs of presumed chemosensory neurons that play distinct roles in chemotaxis are located in the amphid, phasmid and inner labial organs, they either directly or indirectly contact the environment through sensilla openings consisting of glial cells called socket and sheath cell (Fig. Intro3). Additional pair of sensory neurons, AFD are responsible for thermotaxis. Chemosensory system

enables *C. elegans* to detect a wide variety of sensory cues (volatile and water-soluble) associated with food, danger, or other animals (Table. Intro1).

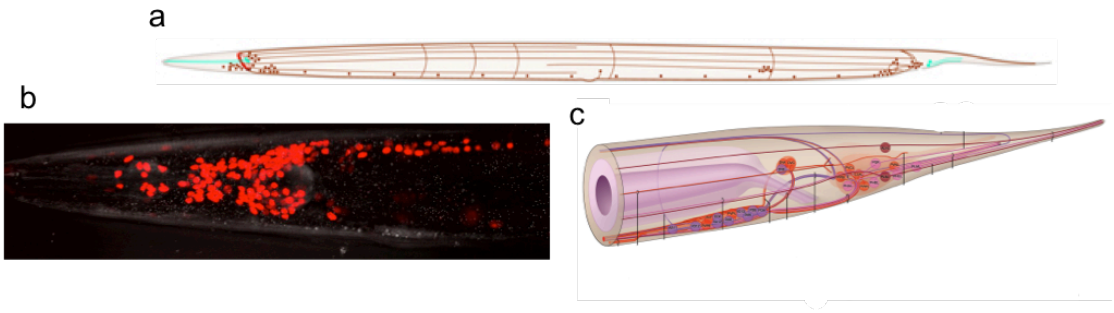

Fig. Intro2. Nervous system of *C. elegans*

a, The whole nervous system of *C. elegans* (Adapted from Wormatlas: http://www.wormatlas.org/hermaphrodite/hermaphroditehomepage.htm). ***b,*** The amphid neurons (This photo was provided by Ms. Kanamori at Iino lab, the strain was *Ex[H20p::NLS4::mCherry]*). The red points are cell nuclei in the head region. ***c,*** Nerve cords and commissures in the tail tip (Adapted from wormatlas: http://www.wormatlas.org/hermaphrodite/nervous/Images/neurofig8leg.htm)

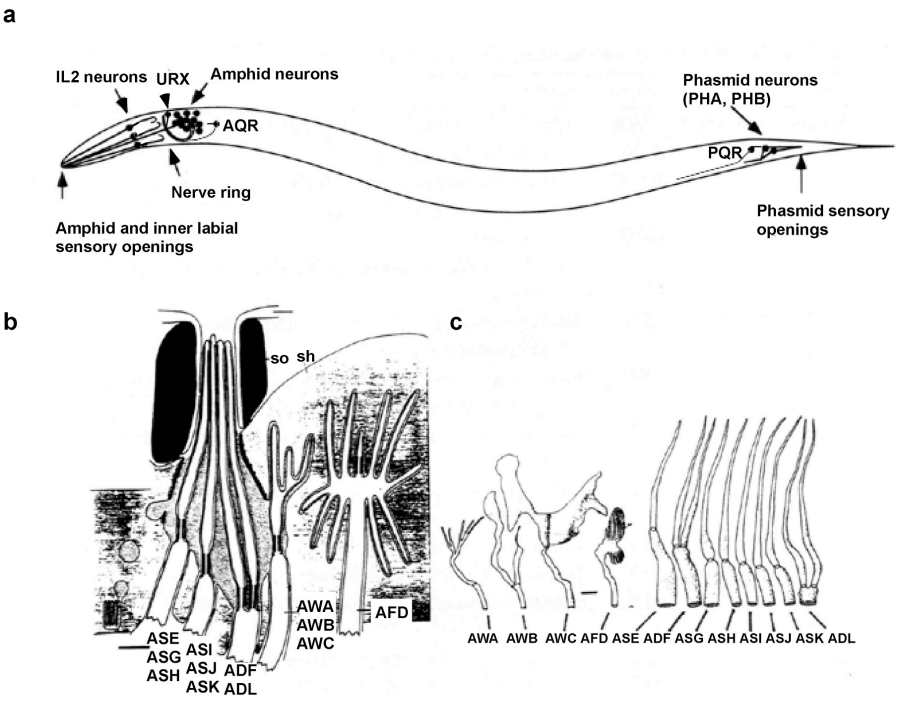

Fig. Intro3. Chemosensory neurons of *C. elegans* (Adapted from Bargmann, 2006).

a, Chemosensory neurons' disposition in *C. elegans*. Each of the two amphids contains 12 associated chemosensory or thermosensory neurons. Each of the two phasmids contains 2 chemosensory neurons, PHA and PHB. ***b,*** The structure and disposition of the amphid sensory opening. It includes ciliated nerve endings, the socket (so), sheath (sh) (Adapted from Perkins et al. (1986)). ***c,*** Detailed structure of the cilia in the 12 classes of amphid neurons (Adapted from Perkins et al. (1986)).

Table. Intro1. Introduction for functions of chemosensory neurons (Adapted from Bargmann, 2006)**.**

Neuron	Function
ASE	Chemotaxis of water-soluble chemicals
AWC	Volatile chemotaxis, Lifespan, Navigation
AWA	Volatile chemotaxis, Lifespan (minor)
AWB	Volatile avoidance
ASH	Nociception: Osmotic avoidance, Nose touch avoidance, Chemical avoidance, Social feeding
ASI	Dauer formation, Chemotaxis(minor), Navigation
ADF	Dauer formation, Chemotaxis (minor)
ASG	Dauer formation (minor), Lifespan, Chemotaxis (minor)
ASJ	Dauer formation and recovery, Chemotaxis (minor), Lifespan
ASK	Avoidance (minor), Chemotaxis (minor), Lifespan, Navigation
ADL	Avoidance (minor), Social feeding
URX, AQR, PQR	Oxygen/aerotaxis, Social feeding
PHA, PHB	Avoidance (antagonistic)

1.3 ASE neurons' functions in chemotaxis of water-soluble chemicals

The pair of ASE neurons is one of the 11 bilateral pairs of amphid chemosensory neurons (Table. Intro1). It is known that the pair of ASE neurons is responsible for sensing water-soluble chemicals judging from the fact that simultaneous ablation of all amphid and phasmid neurons except ASE spares chemotaxis (Bargmann and Horvitz, 1991). The ASE neuron class consists of a bilaterally

symmetrical pair of cells, ASE-left (ASEL) and ASE-right (ASER), which both serve for chemotaxis, but sense different sets of ions. ASEL responds to Mg^{2+}, Li^{+}, and Na^{+}, whereas ASER responds to Br^{-}, I^{-}, and Cl^{-} (Fig. Intro4, Ortiz et al., 2009).

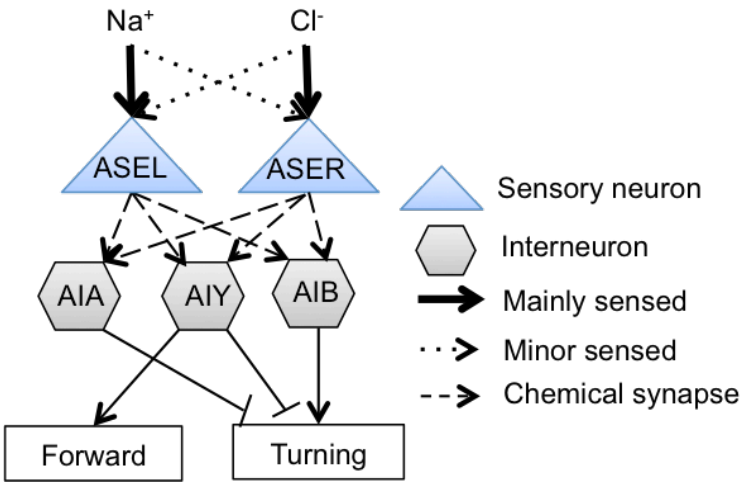

Fig. Intro4. Sensory specificity of ASE salt-sensing neurons and their first layer interneurons.

Property of sensory neurons: Ortiz et al. (2009), connectivity: whites et al. (1986), tole of interneurons: Gray et al. (2005).

C. elegans does not only recognize salt, but also memorizes the salt concentration and move toward or avoid the concentration according to previous experience. When nematodes are grown on a medium that contains salt and food, they show attraction to NaCl by using ASE neurons (Kunitomo et al., 2013). However, when they are starved with NaCl, chemotaxis to NaCl falls dramatically or even becomes aversive (Fig. Intro7, Tomioka et al., 2006; Adachi et al., 2010).

ASEL and ASER neurons have lateralized functions: ASEL neuron is stimulated by increase in salt concentration and promotes forward locomotion, and ASER neuron is stimulated by decrease in salt concentration and promotes either forward or turning behaviors (Fig. Intro4, 5. Suzuki, et al., 2008; Kunitomo et al., 2013).

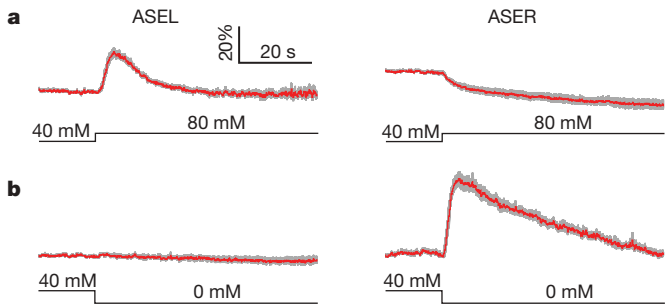

Fig. Intro5. Calcium responses of ASEL and ASER (Adapted from Suzuki et al., 2008) ***a,*** Calcium responses of ASEL and ASER to an upstep of salt concentrations. ***b,*** Calcium responses of ASEL and ASER to a downstep of salt concentrations.

1.4 Behavioral mechanisms for salt chemotaxis

Two behavioral mechanisms have been reported for salt chemotaxis. One is klinokinesis, in which worms regulate the frequency of turning called pirouette, which consists of a bout of sharp turns (Pierce-Shimomura et al., 1999). The other is klinotaxis, in which worms gradually curve towards higher (or lower) salt concentrations (Iino and Yoshida, 2009) (Fig. Intro6). In klinokinesis, worms increase the ratio of pirouette either when salt concentration decreases (driving positive chemotaxis), or when salt concentration increases (driving negative chemotaxis). ASE-ablated mutant shows a severe defect in klinokinesis and klinotaxis, indicating the importance of ASE in the two behavioral mechanisms in salt chemotaxis (Iino and Yoshida, 2009). The Gq/ diacylglycerol (DAG) / protein kinase C (PKC) pathway acts in ASER to promote migration to higher salt concentrations, possibly by augmenting AIB response (Fig. Intro4. Kunitomo et al., 2013). It was also reported that ASER-evoked curving toward lower concentrations by klinotaxis is mediated by AIY interneurons (Fig. Intro4. Satoh et al., 2014).

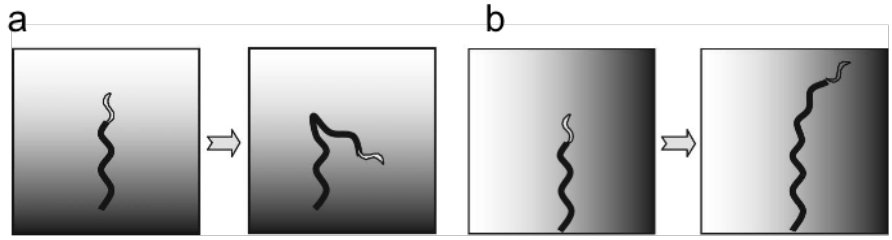

Fig. Intro6. Diagrams of behavioral mechanisms for salt chemotaxis in *C. elegans* (Adapted from Iino and Yoshida, 2009)

a, A diagram of klinokinesis. ***b,*** A diagram of klinotaxis. The shading indicates NaCl gradient.

1.5 ASER's role in salt chemotaxis

1.5.1 ASER's role in salt chemotaxis with food

In ASE neurons, ASER plays an important role in salt chemotaxis (Tomioka et al., 2006; Adachi et al., 2010; Kunitomo et al., 2013). Kunitomo et al. (2013) reported that the ASER-ablated mutant shows a severe defect in salt chemotaxis after cultivation with salt and food, and sensory input only from ASER is sufficient for salt chemotaxis under the condition, indicating ASER plays an important role in salt chemotaxis. *egl-30*, which encodes an ortholog of the alpha subunit of heterotrimetric G-protein Gq, positively regulates locomotory movements (Brundage et al., 1996; Lackner et al., 1999; Adachi et al., 2010). Gq/DAG/PKC signaling pathway in ASER is involved in salt chemotaxis, and promotes migration to higher concentrations (Fig. Intro7, Kunitomo et al., 2013).

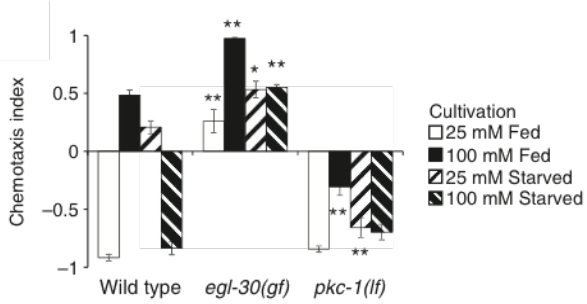

Fig. Intro7. Salt chemotaxis of strains of Gq signal pathway in ASER (Adapted from Kunitomo et al., 2013)]

1.5.2 ASER's role in salt chemotaxis without food

ASER also plays an important role in salt chemotaxis after cultivation without food (Tomioka et al., 2006; Adachi et al., 2010). Adachi et al. (2010) reported that ASEL-ablated mutant showed a small defect in salt plasticity after cultivating in starved conditions (Fig. Intro9), and worms' salt plasticity was mostly, but not fully, dependent on input from ASER, revealing that ASER plays an important role in salt plasticity under starved conditions. Insulin/ phophatidylinositol 3-kinase signaling pathway counteracts the Gq/DAG/PKC signaling pathway and both are involved in salt plasticity under starved conditions (Fig. Intro8, Tomioka et al., 2006; Adachi et al., 2010).

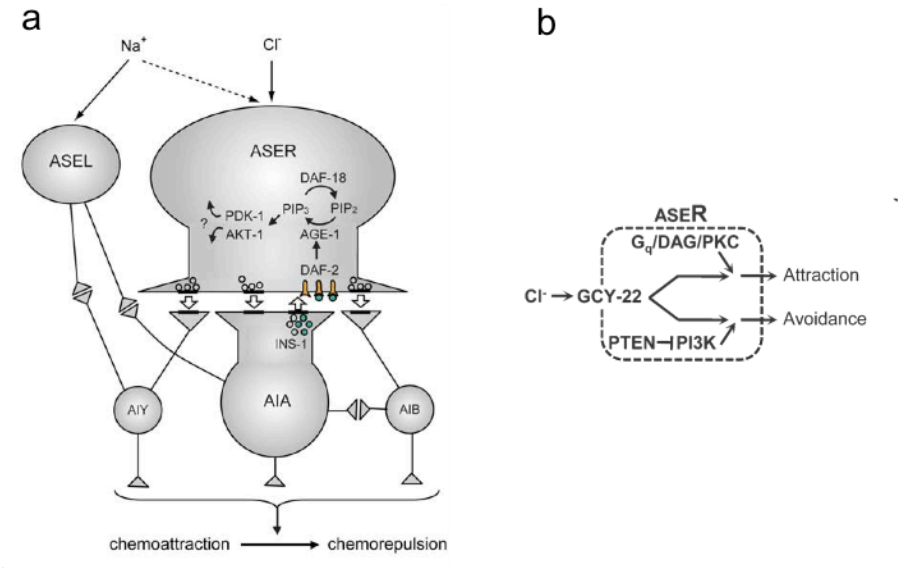

Fig. Intro8. Insulin/PI3K and Gq signal pathway in ASER

a, PI3K signaling pathway in ASER is involved in avoidance behavior in salt chemotaxis (Adapted from Tomioka et al., 2006). ***b,*** PI3K and Gq signal pathway are both involved in salt plasticity (Adapted from Adachi et al., 2010).

1.6 Studies referring to ASEL neuron

1.6.1 Salt chemotaxis

In contrast to ASER, the role and property of the ASEL neuron in salt chemotaxis has not been rigorously examined, although our previous study showed that ASEL was also important for NaCl chemotaxis learning (Fig. Intro9. Adachi et al., 2010). *C. elegans* show salt chemotaxis at relatively low NaCl concentrations typically less than 200 mM (Saeki et al., 2001; Bargmann, 2006; Hukema et al., 2008) like flies (Zhang et al., 2013) and mammals (Chandrashekar et al., 2010). Role of ASE neurons in salt chemotaxis has been well examined at this concentration range. It has been also reported that when ASEL senses a high external concentration of salt (750 mM), it releases INS-6 to AWC neurons to recruit these neurons to act as interneurons for ASEL (Leinwand and Chalasani, 2013).

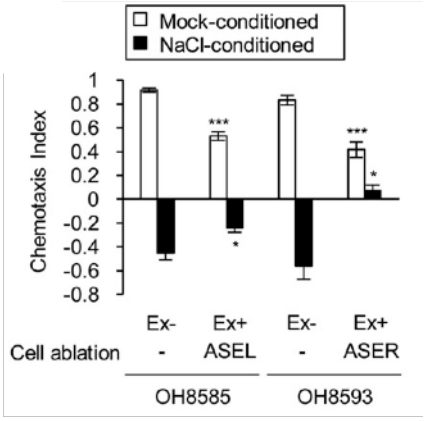

Fig. Intro9. Learning assays were performed with the ASEL-ablated strain (OH8585) and ASER-ablated strain (OH8593). Both strains show impaired learning avoidance but still reveal salt plasticity (Adapted from Adachi et al., 2010)**.**

1.6.2 Other chemotaxis

Compared with few report of ASEL's role in salt chemotaxis, several reports have showed that ASEL, together with ASH, serves as the primary sensor for environmental alkalinity, and plays an essential role for the behavioral response to extracellular alkaline pH (Sassa et al., 2014; Murayama et al., 2013; Murayama and Murayama, 2013; 2015). Besides, in benzaldehyde attraction, it has also been reported that ASEL and AWB act as secondary neurons and receive insulin-like peptides and acetylcholine released by AWC and AWA, respectively

(Leinwand et al., 2015).

1.7 Introduction to intrinsic excitability of neurons

Referring to cellular mechanism for learning and memory in *C. elegans*, so far it usually concerns changes in the strength of synaptic connections in neural circuits for learning or memory storage. However, in other organisms, such as mammals, it has been pointed out that learning and memory are also caused by modifications of the intrinsic properties of a neuron (such as intrinsic excitability). Neuronal excitability can be defined by the tendency of the neuron to generate an output signal (the action potential, AP) in response to a given input signal (usually an excitatory postsynaptic potential, EPSP) (Daoudal and Debanne, 2003). The first report of intrinsic excitability is in a marine mollusk (Alkon, 1984), then a report in *Aplysia* showed that several types of learning are related to persistent changes in neuronal excitability (Cleary et al., 1998). So far, intrinsic excitability has also been reported in mammals (Saar and Baikai, 2009, Gruart et al., 2012; Sehgal et al., 2014), but no report appeared in *C. elegans* so far.

1.8 Development of optogenetics and calcium imaging

1.8.1 Genetically encoded calcium indicators (GECIs) for calcium imaging

The development of fluorescent Ca^{2+} indicators made it possible to measure the Ca^{2+} signals in the cytosol and organelles. There are several types of genetically encoded calcium indicators (GECIs), including reversible and irreversible Ca^{2+} indicators.

1.8.1.1 Irreversible Ca^{2+} indicator, CaMPARI

Irreversible GECIs, also called calcium integrators, were recently constructed.

Fosque et al. (2015) invented CaMPARI (Calcium-modulated photoactivatable ratiometric integrator), a fluorescent sensor, by combining calmodulin (CaM) and its associated M13 peptide (M13) with a photoconvertible green fluorescent protein EosFP. It experiences irreversible green-to-red conversion efficiently upon illumination of violet light only when intracellular Ca^{2+} concentration increased and enables measurement of the calcium activity over large areas of cells and tissues.

1.8.1.2 Reversible GECIs.

Reversible GECIs enable time-lapse monitoring of neuronal activity. Two types of reversible GECIs are widely used: fluorescence resonance energy transfer (FRET)-based GECIs, such as yellow cameleons (Nagai et al., 2004; Horikawa et al., 2010), and GFP-based Ca^{2+} probes. A cp-EGFP-based Ca^{2+} probe called G-CaMP was first reported by Nakai et al. (2001). The N-terminal of cp-EGFP is connected to M13, and C-terminal of cp-EGFP is connected to CAM. Interaction of CAM and M13 by binding of Ca^{2+} triggers conformational change of cp-EGFP, which causes the fluorescence intensity changes. G-CaMPs were widely applied to monitor neuronal activities in nematodes (Oda et al., 2011, Kunitomo et al., 2013), fruitflies (Jayaraman and Lauren, 2007; Yoshihara, 2012), zebrafish (Muto et al., 2011), and mice (Ji et al., 2004; Chen et al., 2012). A series of G-CaMP,, GCaMP1 to GCaMP8 were generated to improve fluorescence intensity and Ca2+ responses (Nakai et al., 2001; Tallini et al., 2006; Tian et al., 2009; Akerboom et al., 2012; Ohkura et al., 2012). Red-colored GECI, RGECO1, which was derived from GCaMP3 (Fig. Intro10, Zhao et al., 2011), expands palette of GECIs. Red-based GECIs, as a new color of GECIs, expanded the palette of GECIs. A series of red-based GECIs, RGECOs and RCaMPs (Ohkura et al., 2012; Wu et al., 2013; Inoue et al., 2015) were developed, and they are comparable to green GECIs in terms of dynamic range, signal-to-noise ratios and kinetics (Walker et al., 2013), and have lower hill coefficient than green GECIs (Table. Intro2, Inoue et al., 2015).

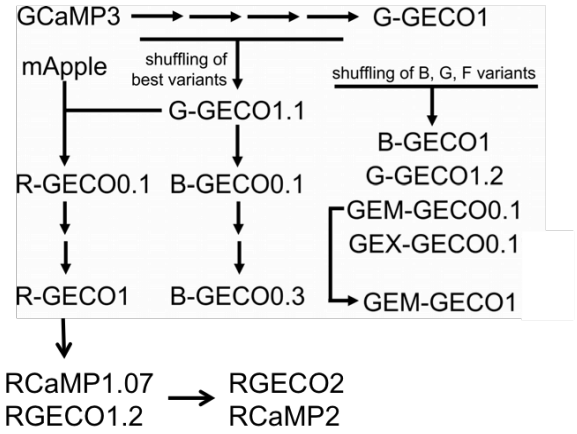

Fig. Intro10. RGECO and RCaMP2 generation. (Based on Zhang et al., 2011)

GECI	$\Delta F/F$	K_d (nM)	Hill coefficient
R-GECO1	8.7 ± 0.7	223 ± 95	2.0 ± 0.2
R-CaMP1.07	14.4 ± 1.4	192 ± 4	1.7 ± 0.1
R-CaMP2	4.8 ± 0.6	69 ± 8	1.2 ± 0.1
R-GECO2L	4.1 ± 0.3	26 ± 3	1.3 ± 0.3
GCaMP3	8.4 ± 0.2	365 ± 8	2.6 ± 0.1
GCaMP5G	18.2 ± 1.0	371 ± 13	2.8 ± 0.2
GCaMP6f	22.1 ± 3.0	296 ± 8	2.1 ± 0.1
GCaMP6s	30.8 ± 3.0	152 ± 8	2.7 ± 0.4

Table. Intro2. Characters of red GECIs and green GECIs. (Adapted from Inoue et al., 2015)

1.8.2 Research progress in optogenetics

Development of optogenetics makes it possible to examine the role of neurons on the behavior by artificially activating or inhibiting particular neurons. Among various opsin genes, channelrhodopsins (ChRs), especially ChR2, are widely used for artificial activation of neurons in optogenetics research (Zhang et al., 2007; Yizhar O, 2011). ChRs are 7-TM proteins capable of conducting passive nonselective cation flow across the cellular membrane upon blue light illumination under the existence of all-trans-retinal (ATR) (Fig. Intro11). Zhang et al. (2007) first applied ChR2 to body wall muscle motor neurons of *C. elegans* to control worms' swimming behavior in vivo. From then on, optogenetics has

been improved rapidly to manipulate neural activity in *C. elegans,* and used to investigate neural functions from synapse level to circuits and behaviors (Husson et al., 2013). Photostimulation of ASER is known to differently regulate klinokinesis turning depending on previous cultivated salt concentrations (Kunitomo et al., 2013). Satoh et al. (2014) reported ASER-AIY neural circuit for klinotaxis in salt chemotaxis using ChR2 expression in AIY or ASER.

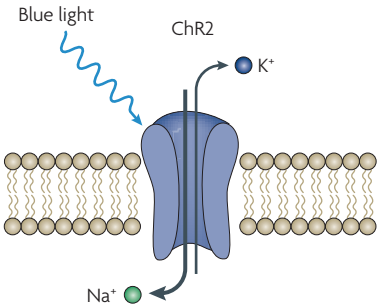

Fig. Intro11. A schematic diagram of ChR2.
ChR2 allows entry of cations into the cell upon illumination with blue light (activation maximus ~470 nm). (Adapted from Zhang et al., 2007).

1.8.3 Combination of optogenetics and calcium imaging

Combination of optogenetics and calcium imaging makes it possible to simultaneously observe behavioral response and dynamic activity of neural circuits induced by manipulation of neuronal activity. Although photoactivation phenomenon is observed in red GECIs, Wu et al. (2013) reported the possibility of combination of ChR2 with Red GECIs for simultaneous optogenetic manipulation and calcium imaging. Ohkura et al. (2012) reported that ChR2-RCaMP1.07 system is applicable for monitoring Ca^{2+} transients in response to optically evoked action potentials and Li et al (2014) applied this system for behavior analysis using non-transgenic animals as the control. Inoue et al. (2015) constructed ChR2-RCaMP2 system and proved that this system is applicable for simultaneous optogenetic manipulation and calcium imaging by using ATR-untreated animals as control (Fig. Intro12).

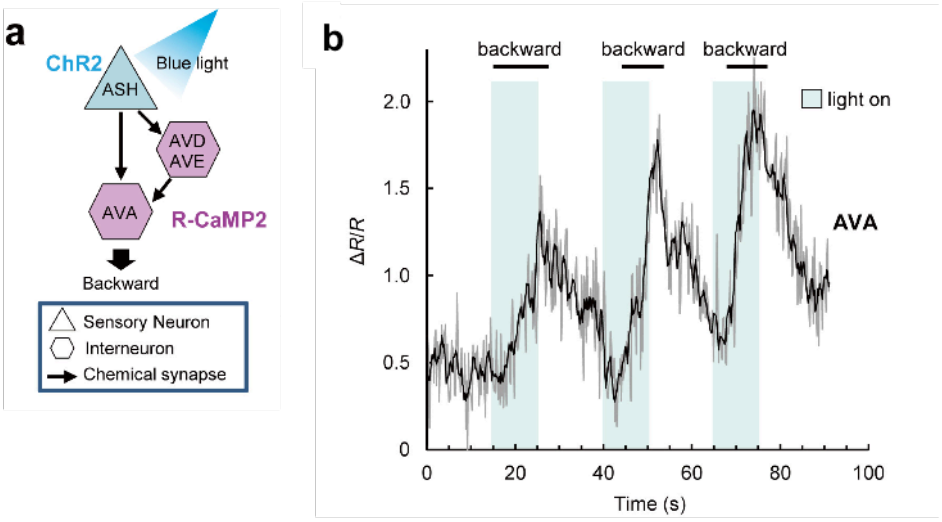

Fig. Intro12. ChR2-RCaMP2-system is applicable to be used in *C. elegans* (Adapted from Inoue et al., 2015).

a, A schema of ChR2-RCaMP2 system expressed in ASH-AVA circuit. ChR2 was expressed in the membrane of ASH sensory neuron and RCaMP2 probe was expressed in AVA motor neuron. ***b,*** Photoactivated of ASH neuron (ChR2 on, light blue shade) causes AVA activation (R-CaMP2, black line in light blue shade) and backward movement (behavioral response).

1.9 The aim of this study

So far, our lab members mainly focused on ASER's role in salt chemotaxis. However, former reports showed that ASEL is also required for worms' salt chemotaxis, thus elucidating the roles of ASEL is crucial to complete understanding of the behavior.

What kind of role does ASEL play in salt chemotaxis? Is ASEL also involved in memory-dependent behavioral plasticity in salt chemotaxis in well-fed conditions? If it is, which interneuron(s) is (are) required for this behavioral plasticity? Optogenetic technology makes it possible to investigate ASEL' role in salt chemotaxis. Using the strain expressing ChR2 in ASEL, worms' behavioral response evoked by activation of ASEL can be observed by illuminating animals under different combinations of cultivation and test salt concentrations.

Besides, since ASEL is a glutamatergic neuron, is glutamate involved in ASEL-generated memory-dependent behavioral response? Gq signaling pathway in ASER plays very important role in salt chemotaxis in well-fed and starved conditions. However, impairment of Gq signal pathway in ASEL showed no or little effect on salt chemotaxis in starved conditions (Adachi et al., 2010). Does Gq signaling pathway in ASEL play a role in ASEL-generated behavioral plasticity in well-fed conditions? I also conducted primary research to answer above two questions.

In this paper, I systematically investigated Na^+ chemotaxis, revealing that ASEL generated a new type of memory-dependent behavioral plasticity in Na^+ chemotaxis. ASEL showed no response after Na^+-free cultivation, but was activated after cultivation with Na^+. Response of the sensory neuron then activate AIY and AIA interneurons to stimulate forward movement, whereas inhibited AIB to prevent turning behavior, both eventually drive worms to higher concentrations. Gq signaling pathway and the neurotransmitter glutamate are both involved in the behavioral response generated by ASEL in Na^+ chemotaxis.

2. Materials and Methods

2.1 Strains

C. elegans strains and transgenic lines used in this study are hermaphrodites and listed in the following table. All *C. elegans* strains were derived from the wild-type strain Bristol N2.

Table M1 *C. elegans* strains and transgenic lines used in this study

Strain	Genotype	Description	Provider
Bristol N2	*C. elegans* wild type	Wild type	CGC
	wIs#3 Is [odr-1(gcy-10)::mCasp, odr-1(gcy-10)::GFP, mec-4::GFP]	Genetic ablation of AWC	Dr.Tokumitsu Wakabayashi
OH9019	*otIs4[gcy-7::gfp]; otEx3822[ceh-36::CZ-caspase3(p17), gcy-7::caspase3(p12)-NZ, myo-3::mCherry]*	Genetic ablation of ASEL	Dr. Oliver Hobert
JN580	*peIs580 [ins-1(short)p::casp1; ins-1(short)p::venus unc-122p::gfp]*	Genetic ablation of AIA	Dr. Hirofumi Sato
JN579	*peIs579 [ttx-3p::casp1 ttx-3p::venus lin-44p::gfp]*	Genetic ablation of AIY	Dr. Hirofumi Sato
JN578	*peIs578 [npr-9p::casp1 npr-9p::venus unc-122p::mCherry]*	Genetic ablation of AIB	Dr. Hirofumi Sato
JN1693	*peIs579 [ttx-3p::mcasp1 ttx-3p::venus lin-44p::gfp]; peIs580 [ins-1(short)p:: mcasp 1 ins-1(short)::venus unc-122p::gfp]*	Genetic ablation of AIY and AIA	Dr. Hirofumi Kunitomo
JN604	*peIs578 [npr-9p::casp1 npr-9p::venus unc-122p::mCherry]; peIs579[ttx-3p::casp1 ttx-3p::venus lin-44p::gfp]*	Genetic ablation of AIY and AIB	Dr. Hirofumi Sato
Jn605	*peIs578 [npr-9p::casp1 npr-9p::venus unc -122p::mCherry]; peIs580[ins-1(short)p ::casp1 ins-1(short)::gfp unc-122p::gfp]*	Genetic ablation of AIB and AIA	Dr. Hirofumi Sato

Strain	Genotype	Description	Provider
JN1694	*peIs578 [npr-9p::mcasp1 npr-9p::venus unc-122p::mcherry]; peIs579 [ttx-3p::mcasp1 ttx-3p::venus lin-44p::gfp]; peIs580 [ins-1(short)p::mcasp1 ins-1(short)::venus unc-122p::gfp]*	Genetic ablation of AIY, AIA and AIB	Dr. Hirofumi Kunitomo
JN1695	*lite-1(ce314) X; peIs1095[gcy7p:: ChR2::venus unc-122p::mCherry]*	Photoactivation of ASEL	Dr. Hirofumi Kunitomo
JN1621	*lite-1(ce314) X; peIs1095[gcy-7p:: ChR2::venus unc-122p::mCherry]; peIs578[npr-9p::casp1 npr-9p::venus unc-122p::mCherry]*	Photoactivation of ASEL under genetic ablation of AIB	Myself
JN1622	*lite-1(ce314) X; peIs1095[gcy-7p:: ChR2::venus unc-122p::mCherry]; peIs579 [ttx-3p::casp1 ttx-3p::venus lin-44p::gfp]*	Photoactivation of ASEL under genetic ablation of AIY	Myself
JN1623	*lite-1(ce314) X; peIs1095[gcy-7p:: ChR2::venus unc-122p::mCherry]; peIs580[ins-1 (short)p::casp1 ins-1(short)p::venus unc-122p::gfp]*	Photoactivation of ASEL under genetic ablation of AIA	Myself
JN1696	*lite-1(ce314) X; Ex[npr-9p::ChR2 unc-122p::mcherry]*	Photoactivation of AIB	Mr. Jun-ichi Tsuchiya
JN1605	*lite-1(ce314) X; Ex[ins-1 (short)p::ChR2 unc-122p::mCherry]*	Photoactivation of AIA	Dr. Yohsuke Satoh
JN1697	*lite-1(ce314) X; Ex[ttx-3p::ChR2 unc-122p::mcherry] (#1)*	Photoactivation of AIY(#1)	Mr. Jun-ichi Tsuchiya
SRS281	*lite-1(ce314) X; pha-1 (e2123) III; sraEx 281[ttx-3p::chop2(H134R):: TagRFP + pBX(pha-1(+))]*	Photoactivation of AIY(#2)	CGC
JN1699	*lite-1(ce314) X; peIs1095 [gcy-7p:: ChR2::venus unc-122p::mCherry]; dyf-11(pe554) X; Ex[gcy-7p::venus::dyf-11(+); myo-3p::Venus]*	Photoactivation of ASEL. ASEL-specific rescue of *dyf-11 (pe554)*.	Myself
JN1698	*lite-1(ce314) dyf-11(pe554) X; peIs1095[gcy-7p::ChR2::venus unc-122p::mCherry]*	Photoactivation of ASEL. *dyf-11(pe554)* background.	Myself
JN1701	*lite-1(ce314) X; peIs1095[gcy-7p:: ChR2::venus unc-122p::mCherry]; Ex [gcy-7::egl-30(Y61N) myo-3p::venus]*	Photoactivation of ASEL. ASEL-specific gain of function of *egl-30*.	Myself

Strain	Genotype	Description	Provider
JN606	*lite-1(ce314) X; Ex[gcy-7p::RGECO lin-44p::gfp]*	Imaging of ASEL.	Myself
JN1624	*lite-1(ce314) X; peIs1095[gcy-7p::ChR2::venus unc-122p::mCherry]; eat-4(ky5)III*	Photoactivation of ASEL. *eat-4(ky5)III* background.	Myself
JN1629	*lite-1(ce314) X; peIs1095[gcy-7p::ChR2::venus unc-122p::mCherry]; Ex[gcy-7p::eat-4(RNAi); myo-3p::venus]*	Photoactivation of ASEL. ASEL specific RNAi of eat-4.	Myself
JN609	*lite-1(ce314) X; peIs1095[gcy-7p::ChR2::venus unc-122p::mCherry]; Ex[npr-9p::Rcamp2; lin-44::gfp]*	Imaging of AIB under photoactivation of ASEL	Myself
JN610	*lite-1(ce314) X; peIs1095[gcy-7p::ChR2::venus unc-122p::mCherry]; Ex[ttx-3p::Rcamp2; lin-44::gfp]*	Imaging of AIY under photoactivation of ASEL	Myself
JN608	*lite-1(ce314) X; peIs1095[gcy-7p::ChR2::venus unc-122p::mCherry]; Ex[ins-1p::RGECO; lin-44::gfp]*	Imaging of AIA under photoactivation of ASEL	Myself
JN607	*lite-1(ce314) X; peIs1095[gcy-7p::ChR2::venus unc-122p::mCherry]; Ex[gcy-7p::RGECO1; lin-44::gfp]*	Imaging of ASEL under photoactivation of ASEL	Myself
JN611	*lite-1(ce314) X; peIs1095[gcy-7p::ChR2::venus unc-122p::mCherry]; Ex[gcy-7p::RCaMP2; lin-44::gfp]*	Imaging of ASEL under photoactivation of ASEL	Myself

2.2 Culture of *C. elegans*

2.2.1 Composition of growth medium and buffer

Nematode growth medium plates (NGM plates)

2.5 g/L Hypolypepton

3 g/L NaCl

17 g/L Agar

1 ml/L cholesterol (5 mg/ml in EtOH)

Autoclaved at 121 ^{o}C for 20 min, and then added the following and mixed after each addition through sterile technique.

25 mM Potassium phosphate (pH 6.0)

1 mM $CaCl_2$

1 mM $MgSO_4$

The hot (~50°C) agar (10 ml) was poured into 6 cm plates. They are stocked at room temperature for two days, and then moved into refrigerators (4°C) for usage.

M9 Buffer

0.3 % KH_2PO_4

1.51 % $Na_2HPO_4/12H_2O$

0.5 % NaCl

1 mM $MgSO_4$

Autoclave.

2.2.2 Food Source of *C. elegans*

Fast-growing *E. coli* NA22 was used as food source in behavioral assays and chemotaxis assays to avoid starvation (Tomioka et al., 2006; Adachi et al., 2010; Kunitomo et al., 2013). OP50 was used for imaging experiments because animals cultivated with NA22 tended to exhibit high background fluorescence in the intestine (Oda et al., 2011; Kunitomo et al., 2013).

2.2.3 Cultivation

All animals were cultivated at 20 °C under standard conditions (Brenner, 1974) except for SRS281 (Table. 1), which was cultivated at 25°C as described by Kocabas et al., 2012 and Satoh et al., 2014.

2.3 Chemotaxis assay.

2.3.1 Compositions of plates and buffers for chemotaxis assay

Pre-assay cultivation NGM plates (0 mM/100 mM)

2.5 g/L Hypolypepton

17 g/L Agar

1 ml/L cholesterol (5 mg/ml in EtOH)

0/100 mM NaCl

Autoclaved at 121 ^{o}C for 20 min, and then axenically supplemented with the followings.

25 mM Potassium phosphate (pH 6.0)

1 mM $CaCl_2$

1 mM $MgSO_4$

The molten (~50^{o}C) agar (10 ml) was poured into a 6 cm dish. Plates were left at room temperature overnight, and stored at 4^{o}C.

Assay plates for Na^+ chemotaxis

100 mM NH_4Cl (pH6.0)

2% Bacto agar

Autoclaved at 121 ^{o}C for 20 min, and then axenically supplemented with the followings.

25 ml Potassium phosphate (pH 6.0)

1 ml $CaCl_2$

1 ml $MgSO_4$

The molten (~50^{o}C) agar (10 ml) was poured into a 9 cm dish. Plates were left at room temperature overnight, and stored at 4^{o}C.

Plug plates for Na^+ chemotaxis

100 mM NH_4Cl plug plates (Compositions were the same as assay plates)

100 mM NaCl plug plates

100 mM NaCl

2% Bacto agar

Autoclaved at 121 °C for 20 min, and then axenically supplemented with the followings.

25 mM Potassium phosphate (pH 6.0)

1 mM $CaCl_2$

1 mM $MgSO_4$

The molten (~50°C) agar (30 ml) was poured into a 9 cm dish. Plates were left at room temperature overnight, and stored at 4°C.

Wash buffer

0/50/100 mM NaCl

0.05 % gelatin

Autoclaved at 121 °C for 20 min, and then axenically supplemented with the followings.

25 mM Potasium phosphate (pH 6.0)

1 mM CaCl2

1 mM MgSO4

2.3.2 Na^+ chemotaxis assay

2.3.2.1 The procedure to form Na^+ gradient

To evaluate animals' behaviors on Na^+ gradient, a modified chemotaxis assay was used in this study. Assay plates were prepared as shown in Figure M1. 100 mM NH_4Cl (pH6.0) assay plates stored at 4 °C were warmed to room temperature (22 °C). Two cylindrical agar blocks excised from plug plate (each 14.5 mm in diameter, either 100 mM NaCl (A site) or 100 mM NH_4Cl (B site)) (Fig. M1a), were placed on the NH_4Cl (pH6.0) assay plates at 20 °C for 24 h and removed just before assay. This procedure created a concentration gradient on the assay plate with a Na^+ concentration of 45 mM at point A, 5 mM at point C, and 0 mM at point B (Fig. M1b) and a NH_4^+ concentration of 65 mM at point A, 95 mM at point C, and 100 mM at point B (Fig. M1c), based on a numerical simulation of diffusion

(Iino and Yoshida et al., 2009; Kunitomo et al., 2013).

2.3.2.2 Procedures for Na^+ chemotaxis

Animals were grown to young adults on standard NGM plates, and then transferred to pre-assay cultivation NGM plates either without Na^+ or with 100 mM Na^+ for 6 h. One- to two-hundred animals were washed out from the plates and placed at the center of assay plates (C point) (Fig. M2). One microliter each of 0.5 M NaN_3 was spotted on points A and B of assay plates just before the start of each assay. After nematodes were allowed to move for 45min, the assay plates were chilled at 4 °C before counting. Animals within a 2 cm radius from the center of each agar block were considered to be attracted, and animals within a 1cm radius from the start point were excluded from the total number of animals to calculate chemotaxis index.

$$\text{Chemotaxis Index} = \frac{\text{Number of worms at A area} - \text{Number of worms at B area}}{\text{all number of worms on the plates} - \text{Number of worms at C area}}$$

$$\text{Movement index} = \frac{\text{Number of worms at A area} + \text{Number of worms at B area}}{\text{all number of worms on the plates}}$$

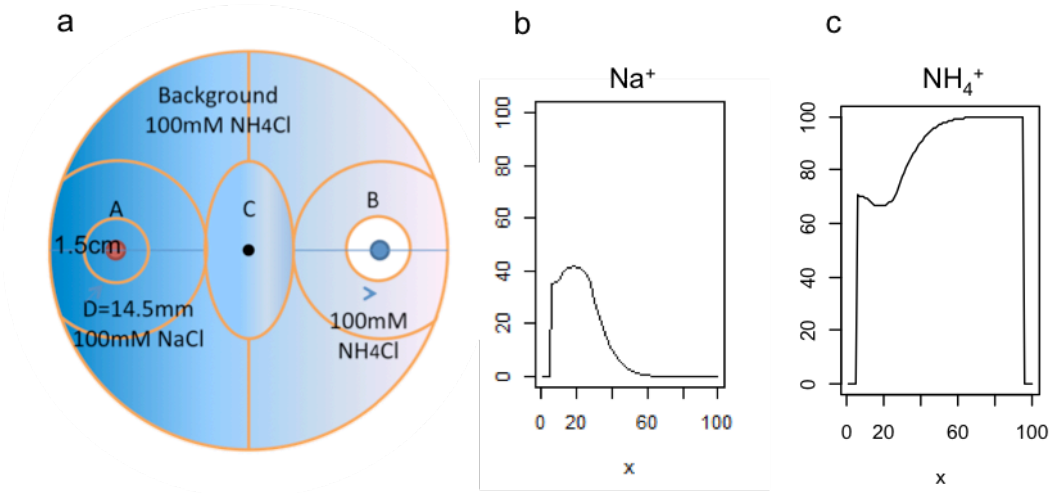

Figure. M1 Assay plate format for Na^+ chemotaxis assay.

a, The schematic format of assay plate to generate a cation gradient on a test plate; ***b*** & ***c***, Concentrations of Na^+ (***b***) and NH_4^+ (***c***) from A area to B area of assay plate (***a***) after 24 h.

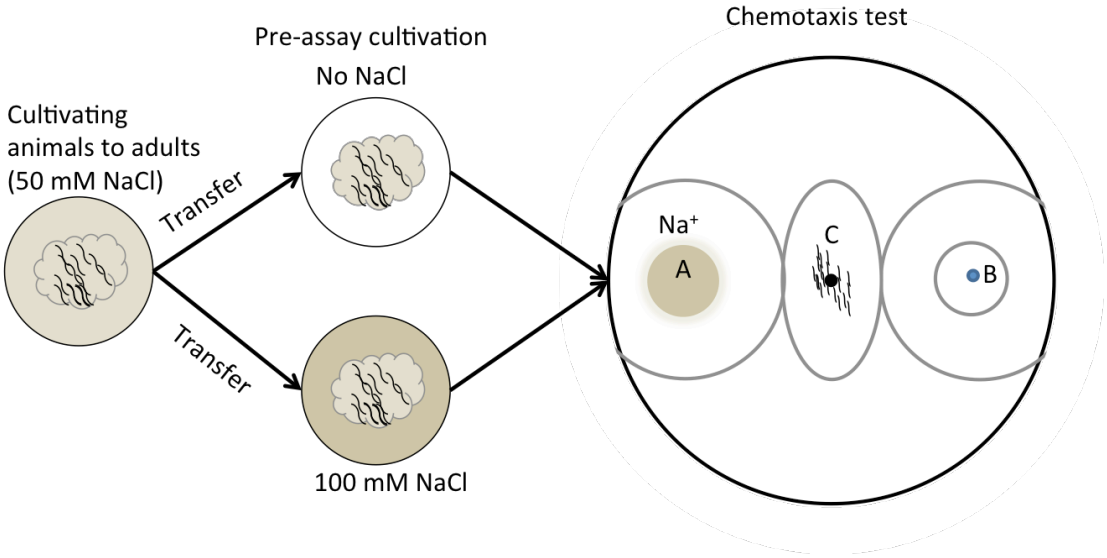

Figure. M2 The procedure for Na^+ chemotaxis

2.4 Optogenetic stimulation and behavioral assay.

2.4.1 Compositions of plates and buffers for behavioral assay

Assay plates with different NaCl (NaAc) concentrations

0/25/50/100 mM NaCl or 25/50 mM NaAc

2 % Bacto agar

Autoclaved at 121 °C for 20 min, and then axenically supplemented with the followings.

25 mM Potassium phosphate (pH 6.0)

1 mM $CaCl_2$

1 mM $MgSO_4$

The molten (~50°C) agar (10 ml) was poured into a 9 cm dish. Plates were left at room temperature overnight, and stored at 4°C.

Pre-assay cultivation NGM plates with different NaCl (NaAc) concentrations

0/25/50/100 mM NaCl or 25 mM NaAc

2.5 g/L Hypolypepton

17 g/L Agar

1 ml/L cholesterol (5 mg/ml in EtOH)

Autoclaved at 121 °C for 20 min, and then axenically supplemented with the followings.

25 mM Potassium phosphate (pH 6.0)

1 mM $CaCl_2$

1 mM $MgSO_4$

The molten (~50°C) agar (10 ml) was poured into a 6 cm dish. Plates were left at room temperature overnight, and stored at 4°C.

Wash buffer with different NaCl concentrations (The same as 2.3.1)

2.4.2 Pre-assay cultivation

2.4.2.1 Preparation of pre-assay cultivation NGM plates

2.4.2.1.1 Liquid cultivation of NA22 strain of *E.coli*

A single colony-derived *E.coli* NA22 cells were propagated in 5 ml of LB at 37 °C overnight and stored at 4 °C until use.

2.4.2.1.2 Preparation of pre-assay cultivation NGM plates

NA22 suspension (1 ml) was added to a microtube that contained 10 μL of 100 mM all-trans retinal (ATR, Sigma) and well mixed, 100 μL each of the mixture was spread on a pre-assay cultivation NGM plate (finally 10 μM ATR), and plates were packaged by aluminum foil paper, then cultivated at 37 °C for one to two days until dried, and then stored at 4 °C until use. Control plates were similarly prepared without ATR.

2.4.2.2 Pre-assay cultivation of worms

Young adults grown on standard NGM plates were further cultivated with food under various salt concentrations suspended with ATR (10 μM) overnight. Worms cultivated under various salt concentrations without ATR were used as controls.

2.4.3 Multi-worm tracking system

Multi-worm tracking system consisted of the following equipments (Fig. M3): A ring-shaped light-emitting diode (LDR2-90BL, CCS) used for applying blue light stimulation, another ring-shaped white light (HPR-150SW, CCS) placed around the blue light, a CCD camera (LW575C, ARGO) for tracking worms' locomotion, and a software called "LuCam Tracker 1.7.8" for analysis of worms' behavior.

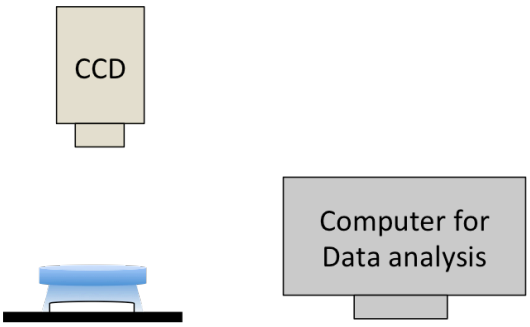

Fig. M3 Multi-worm tracking system.

2.4.4 Behavioral assay

Worms' behavior was tested on assay plates without salt gradient. Animals were placed on the test plate and left for 2 min. Pulses of blue light (peak wavelength 470 nm; ~0.2mW/mm^2) whose duration range from 1s to 60 s depending on experiments were applied. Each animal was applied 5 photostimulations with 80 s intervals. Locomotion was monitored by LuCam Tracker 1.7.8. At least 6 independent experiments were performed for each condition.

2.4.5 Data analysis

The turning event rate was calculated as the ratio of animals that were during pirouettes, sharp turns or pauses (collectively called turning events) at each time point. The average turning events rate of a 21 s window before stimulation (typically, time -30 s to -10 s) was calculated and termed as NS (No stimulation); the average turning events rate of a 5 s window (3 s for AIY#1 (Figs. 8c; 26e)) during stimulation (typically, Time 3 s–7s (2 s-4 s for AIY#1)) was calculated and termed as DS (during stimulation); change of turning events rate during stimulation (CDS) was calculated by subtracting NS from NS.

2.5 Optogenetic stimulation and calcium imaging.

2.5.1 Compositions of plates and buffers for behavioral assay

Pre-cultivation plates with different NaCl concentrations (The same as 2.4.1)
Imaging solution with different NaCl concentration (The same as 2.3.1)

2.5.2 Pre-assay cultivation

2.5.2.1 Preparation of pre-assay cultivation NGM plates

(The same as 2.4.2.1 except that NA22 was replaced by OP50)

2.5.2.2 Pre-assay cultivation of worms

Animals were cultivated on NGM plates until young adults and further cultivated overnight on pre-assay cultivation NGM plates (see 2.5.2.1) with or without Na^+ (50 mM). Then an animal was immobilized in a microfluidic device (Fig. M4, Chronis et al., 2007) with imaging solutions (50 mM NaCl for worms cultivated without Na^+ and 100 mM NaCl for worms cultivated with 50 mM Na^+).

2.5.3 Generation of transgenic animals

2.5.3.1 Plasmid construction.

2.5.3.1.1 pENTR plasmid

pENTR plasmids used in this research have been made by lab members previously (Table. M2).

Table. M2 pENTR information

The name of plasmid	Expressing cells	Provider
pENTR-gcy-7p	ASEL	Dr. Masahiro Tomioka
pENTR-ttx-3p	AIY	Prof. Yuichi Iino
pENTR-ins-1p	AIA, (part of intestine)	Dr. Koji Yamada
pENTR-npr-9p	AIB	Dr. Shigekazu Oda

2.5.3.1.2 pDEST plasmid

pDEST-RGECO was a gift from Prof. Takeshi Ishihara (Kyushu University) and *pDEST-RCaMP2* was kindly provided by Dr. Keiko Gengyo-Ando (Saitama University, Japan), Prof. Junichi Nakai (Saitama University, Japan), and Prof. Haruhiko Bito (The University of Tokyo).

2.5.3.1.3 Plasmid construction

Plasmids for germline transformation were generated by the Gateway system (Invitrogen) in which the LR reaction was used to combine the promoter sequence on an entry vector and the ORF of the gene of interest on a destination vector.
Details of this method have been described clearly in the Homepage of Iino lab:
http://molecular-ethology.biochem.s.u-tokyo.ac.jp/Gateway/Gateway_overview1_jp.html

pG[gcy-7p::RcaMP2], *pG[gcy-7p::RGECO]*, *pG[ttx-3p::R-CaMP2]*, *pG[ins-1(short)p::RGECO]*, *pG[npr-9p::R-CaMP2]*, were produced.
pG[lin-44::gfp] is a gift from Ishihara lab.

2.5.3.2 Microinjection

According to previous instruction (Mello et al., 1991), the following DNA mixtures were microinjected to ASEL-ChR2 strain: *lite-1(ce314) X; peIs1095[gcy7p:: ChR2Y2::venus unc-122p::mCherry]*

pG[gcy-7p::RcaMP2] (76.7 ng/μL)
pG[lin-44::gfp] (19.5 ng/μL)
→ *lite-1(ce314) X; peIs1095[gcy7p:: ChR2Y2::venus unc-122p::mCherry]; Ex[gcy-7::RCaMP2; lin-44::gfp]*

pG[gcy-7p::RGECO] (94.4 ng/μL)
pG[lin-44::gfp] (13.0 ng/μL)
→ *lite-1(ce314) X; peIs1095[gcy7p:: ChR2Y2::venus unc-122p::mCherry]; Ex[gcy-7p::RGECO; lin-44::gfp]*

pG[ttx-3p::R-CaMP2] (72.5 ng/μL)
pG[lin-44::gfp] (13.0 ng/μL)
→ *lite-1(ce314) X; peIs1095[gcy7p:: ChR2Y2::venus unc-122p::mCherry]; Ex[ttx-3p::RCaMP2; lin-44::gfp]*

pG[ins-1(short)p::RGECO] (94.2 ng/μL)
pG[lin-44::gfp] (26.1 ng/μL)
→ *lite-1(ce314) X; peIs1095[gcy7p:: ChR2Y2::venus unc-122p::mCherry]; Ex[ins-1(short)p: :RCaMP2; lin-44::gfp]*

pG[npr-9p::R-CaMP2] (56.9 ng/μL)
pG[lin-44::gfp] (18.4 ng/μL)
→ *lite-1(ce314) X; peIs1095[gcy7p:: ChR2Y2::venus unc-122p::mCherry]; Ex[npr-9p::RCaMP2; lin-44::gfp]*

2.5.4 Optogenetic and calcium imaging system

Optical stimulation during calcium imaging were performed on a fluorescent microscope system as previously described (Satoh et al., 2014) with modifications (Fig. M4). I used an upright microscope (BX51, Olympus) equipped with a halogen light source (U-LH100IR), a UplanApo 40x objective (NA, 0.85), 530/50 nm band-path excitation filter and DV2 photometrics (DV2-cube, T565 lpxr, Olympus), a motorized stage (HV-STU02-1, HawkVision), a CCD camera (GRAS-03K2M-C, point Grey Research) and a blue LED (470 nM, PE-100, CollLED) for worm observation and stimulation at 4 frames/s (exposure time: 50 ms).

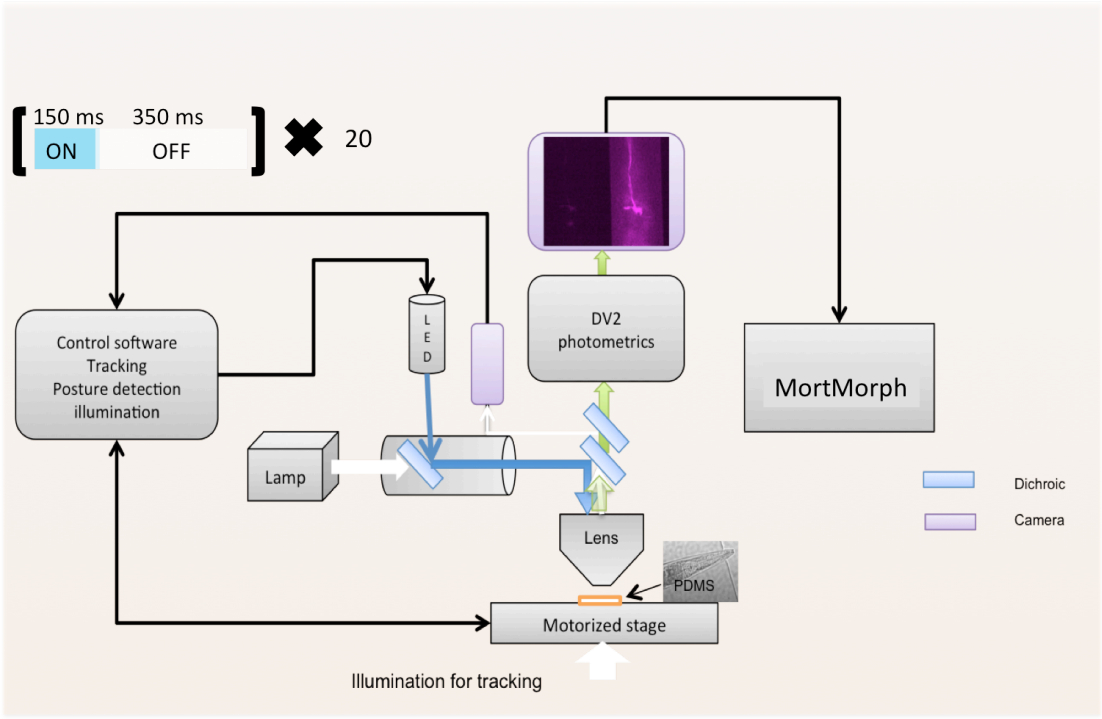

Fig. M4 Schematic drawing of optogenetic and calcium imaging system that enables LED stimulation at regular intervals

2.5.5 Calcium imaging under photoactivation

In each experiment, recording of calcium imaging was initiated 5 min after removal of animal from pre-assay cultivation plates. Individual animals were

subjected to a single recording and replaced for each experiment. Regulated photostimulation was started after 20 s recording and consisted of 20 cycles of 150 ms stimulations with 350 ms intervals (10 s in total).

2.5.6 Data acquisition and analysis

Fluorescence images obtained during the 350 ms intervals were used for quantification. Average fluorescence intensity of the neurons (cell body for ASEL; dendrites for AIB, AIY, and AIA) was calculated from the region of interest, whose position was automatically followed using the Track Objects function of Metamorph software (Molecular devices) followed by subtraction of the average intensity of the background region. The average fluorescence in a 10 s window (typically, time 11 s–20 s (41-80 frame)) was set as F_0 and the fluorescence intensity relative to F0 (F/F0) was calculated for a series of images. For each figure, F/F_0 was averaged for all animals at each time point. The average F/F_0 in a 5 s window before stimulation (typically, Time 3 s–7 s) was set as NS (No stimulation); the average F/F_0 in a 5 s window during stimulation (typically, Time 13 s–17 s (16 s-10 s for AIB (Fig. 17))) was set as DS (during stimulation); F/F_0 change during stimulation equals DS subtracted by NS.

3. Results

3.1 ASEL generates memory-dependent behaviors in Na^+ chemotaxis

3.1.1 A behavioral test for Na^+ chemotaxis

To test worms' chemotaxis to Na^+, I devised a chemotaxis assay using an agar plate in which Na^+ and NH_4^+ make reciprocal concentration gradients (Fig. M1b&c). It has been reported that AWC neurons are responsible for NH_4^+ chemotaxis (Frøkjær-Jensen et al., 2008). However, in the Na^+ chemotaxis test, AWC-ablated mutants showed chemotaxis that was comparable to that of wild type, indicating that NH_4^+ gradient does not largely affect Na^+ chemotaxis in this assay plate format (Fig. 1). Thus, this assay is adequate to evaluate Na^+ chemotaxis.

3.1.2 Worms show behavioral plasticity in Na^+ chemotaxis

Na^+ chemotaxis assay was performed using animals cultivated under different salt conditions. Animals cultivated under Na^+-free conditions, showed no Na^+ concentration preference, whereas those cultivated under the presence of 100 mM NaCl showed positive Na^+ chemotaxis (*i. e.* migration to higher Na^+ concentrations, Fig. 1). ASEL-ablated mutant showed a defect in Na^+ chemotaxis, indicating the important role of ASEL in Na^+ chemotaxis.

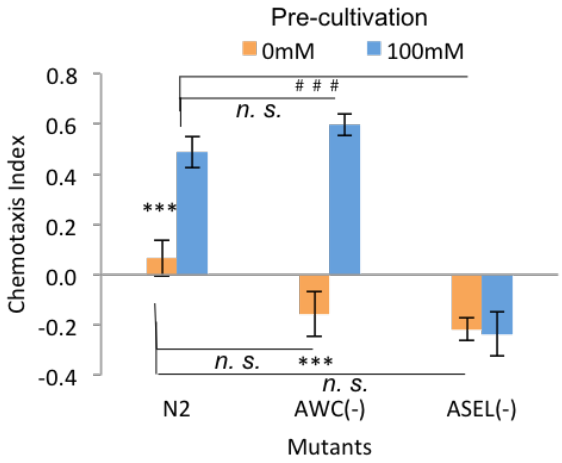

Fig. 1 Worms showed behavioral plasticity in Na^+ chemotaxis.

Na^+ chemotaxis of wild type N2, AWC-ablated and ASEL-ablated strains after 0 or 100 mM NaCl cultivation (mean ± s.e.m., n ≥ 7, *n.s.*, no significant difference, ***$p < 0.001$). The cultivation concentrations have significant effect on chemotaxis index: $F_{(2, 34)} = 13.08$, $p < 0.0001$; the neuronal cell-ablated strains have significant influence in chemotaxis index: $F_{(1, 34)} = 22.80$, $p < 0.0001$; the interaction between neuronal cell-ablated strains and cultivation concentrations is considered significant: $F_{(2, 34)} = 11.92$, $p = 0.0001$; two way ANOVA.

3.1.3 Forward locomotion is promoted by stimulation of ASEL after cultivation with Na^+

Although ASEL is known as the major Na^+-sensing neuron, ASER also contributes to Na^+ chemotaxis to a lesser extent (Fig. Intro4, Ortiz et al., 2009). In addition, ASER plays a major role in the behavioral plasticity of NaCl chemotaxis probably through its Cl^--sensing functions (Tomioka et al., 2006; Adachi et al., 2010; Kunitomo et al., 2013). Therefore, I decided to focus on the ASEL's role in Na^+ chemotaxis by employing optogenetics combined with a behavioral assay and calcium imaging.

3.1.3.1 ASEL photoactivation to artificially imitate increasing Na^+ concentrations

Transgenic worms, in which channelrhodopsin (ChR2) was expressed only in ASEL, were illuminated by blue light after pre-assay cultivation at different NaCl concentrations and the behavioral response was quantified by the worm-tracking system. Since ASEL is activated by an increase in Na^+ concentrations, optogenetic activation of ASEL mimics sensation of an increase of Na^+ concentrations. I evaluated the behavioral response by calculating the truning events, which was the ratio of animals that were during pirouettes, sharp turns or pauses (collectively called turning events in this manuscript) at each time point. Therefore, the event rates roughly equal one subtracted by the rate of forward locomotion.

3.1.3.2 Promotion of forward locomotion by ASEL photoactivation after cultivation with Na^+

When worms were cultivated with Na^+ and tested on test plates at any Na^+ concentration (even without Na^+), the ratio of turning events decreased (forward locomotion was stimulated) during blue-light illumination and increased after illumination (Fig. 2a-b). These results are similar to the previous observation of behavioral responses to NaCl concentration change, in which animals decrease or increase turning upon up-step or down-step of NaCl concentration, respectively (Miller et al., 2005). Such behavioral response can generate chemotaxis to a higher salt concentration through the klinokinesis mechanism. These results were consistent with the observation that worms cultivated with Na^+ migrated to a higher concentration (Fig. 1&2c).

It was noted that decreases in turning rate on 100 mM Na^+ test plates were larger than those on 50 mM or 0 mM plates (Fig. 2c). It is suggested that worms showed improved behavioral response upon ASEL photoactivation at high Na^+ concentrations after cultivation with Na^+.

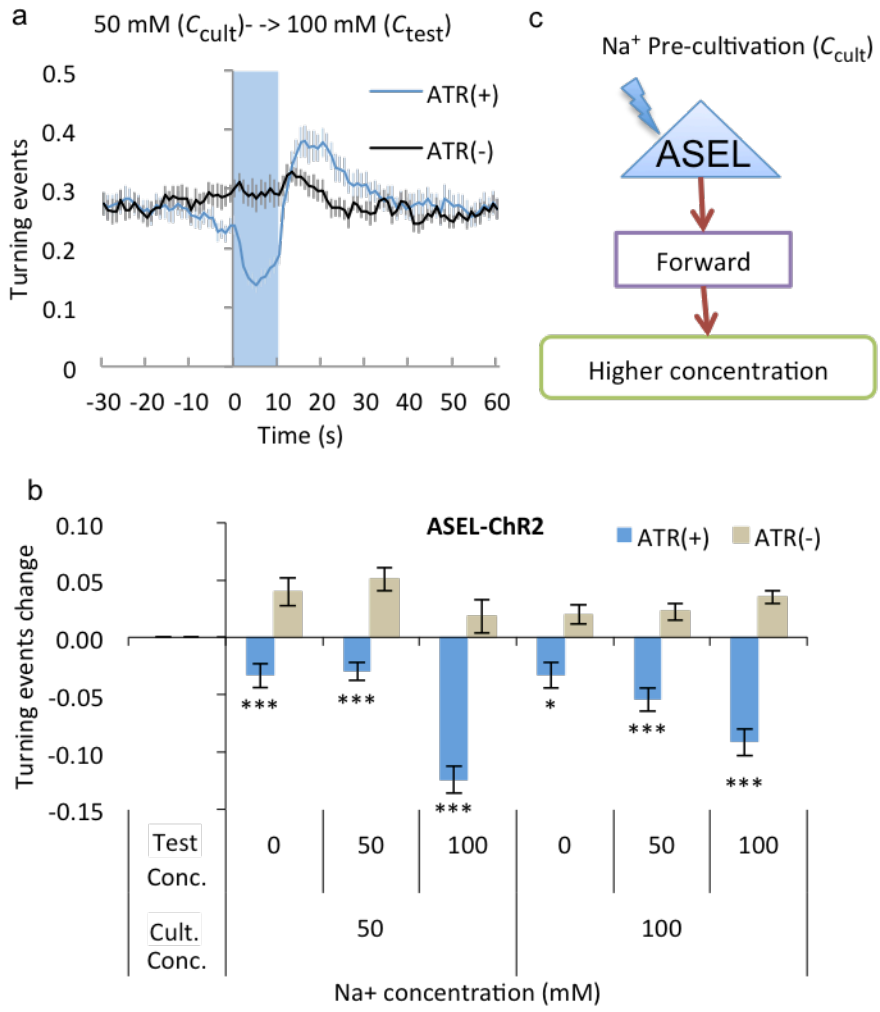

Fig. 2 Worms' behavioral response upon ASEL photostimulation after cultivation with Na⁺

a, Ratio of turning events evoked by optical stimulation of ASEL (blue vertical shading) tested at 100 mM Na⁺ (*C*test) after cultivation at 50 mM Na⁺ (pre-assay cultivation, *C*cult) (mean ± s.e.m., n ≥ 12). ***b,*** Change of turning event rate of worms during ASEL photostimulation at different cultivation and test concentrations (see Material and methods) (mean ± s.e.m., n ≥ 12). Difference between ATR (+) and ATR (-): $F_{(11, 150)}$ = 29.936, $p < 0.0001$; $k = 6$, *$kp < 0.05$, *** $kp < 0.001$, one-way ANOVA followed by *t-test* with Bonferroni's correction. For the ATR (+) conditions, the test concentrations have significant effect on behavioral response: $F_{(2, 81)} = 30.53$, $p < 0.0001$; the cultivation concentrations have nonsignificant effect on behavioral response: $F_{(1, 81)} = 0.03$, $p = 0.8733$; the interaction between test concentrations and cultivation concentrations is considered significant: $F_{(2, 81)} = 3.35$, $p = 0.0401$; two way ANOVA. ***c,*** The model of ASEL which generates forward locomotion after cultivation with Na⁺.

3.1.4 Worms' behavioral responses upon ASEL photoactivation in different strengths

The ration of turning events was unchanged by stimulation of ASEL if animals were cultivated on Na^+-free medium irrespective of stimulus intensity (Fig. 3a). On the other hand, inhibition of turning of Na^+-conditioned animals was enhanced according to the stimulus intensity (Fig. 3b), which is consistent with the previous reports about photoactivation of AIY (Li et al., 2014) and AWA (Larsch et al., 2015) that stronger stimulation strengths leads to bigger behavioral responses.

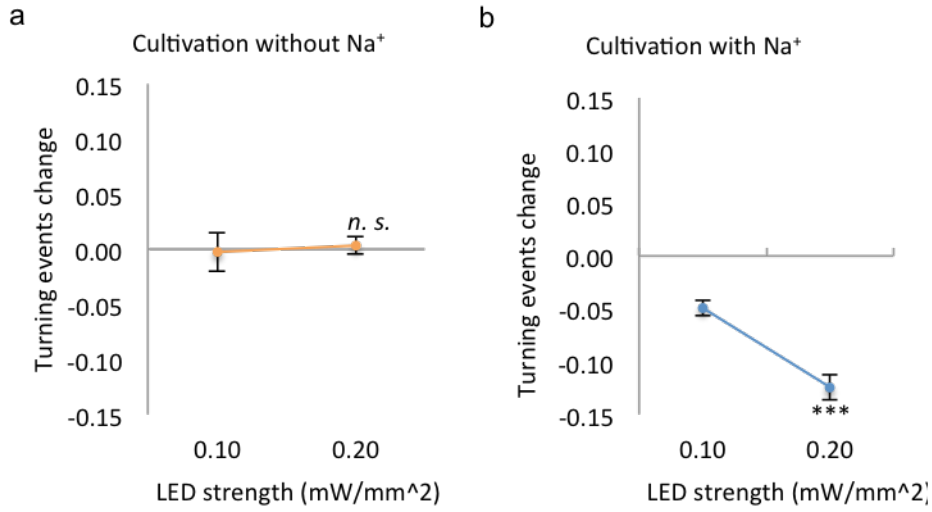

Fig. 3 Worms' behavoiral responses to ASEL photostimulation with different stimulus intensity.

Change of turning event rate upon ASEL phtostimulation under different stimulation strengths after cultivation without Na^+ (a) and with Na^+ (b) (mean ± s.e.m., n ≥ 12, ***p < 0.001, *n. s.* no significant difference, student *t-test*, significant difference between different LED strengths). ***a,*** worms' turning events change to ASEL photoactivation when worms were tested at 50 mM Na^+ after Na^+-free cultivated condition with ATR. ***b,*** worms' turning events change to ASEL photoactivation when worms were tested at 100 mM Na^+ after cultivation at 50 mM Na^+ with ATR.

3.1.5 Worms' behavioral response upon ASEL photoactivation at different time lengths

Several reports show that optogenetic sensitivities vary among cell types in *C. elegans*. For example, Zhang et al. (2007) reported worms can behaviorally respond to 1 s photoactivation when ChR2 was expressed in muscle cells. On the other hand, ASH requires 10 s photoactivation for generating a behavioral response (Guo et al., 2009). Kunitomo et al. (2013) reported that ASER shows behavioral response by only 1 s photoactivation, whereas AIB needs 3s. According to our results, ASEL was not so sensitive than ASER, worms showed no behavioral response by 1 s photoactivation. However, after cultivation with Na^+, worms showed decrease of turning events upon 10 s photostimulation, and prolonged stimulation caused no change in worms' behavioral pattern (Fig. 4), which was also the case in former reports on photoactivation of AIY (Li et al., 2014) and AWA (Larsch et al., 2015). Even prolonged stimulation did not generate any behavioral response if animals were cultivated without Na^+ (Fig. 3a&4).

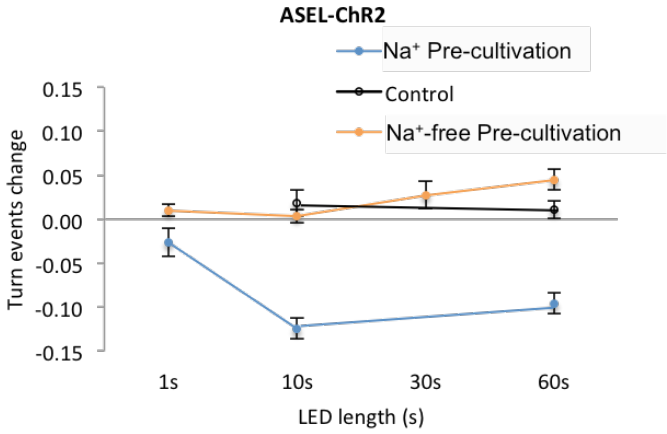

Fig. 4 Change of turning events upon ASEL's photoactivation at different duration (mean ± s.e.m., n ≥ 6).

Orange line shows worms' turning events change upon ASEL photoactivation when worms were tested at 50 mM Na^+ after Na^+-free cultivation with ATR. Blue line shows worms' turning events change upon ASEL photoactivation when worms were tested at 100 mM Na^+ after 50 mM Na^+ cultivation with ATR. Black line shows worms' turning

events change upon ASEL photoactivation when worms were tested at 100 mM Na^+ after cultivation at 50 mM Na^+ without ATR.

3.2 AIB is required for Na^+ chemotaxis after cultivation with Na^+

AIB, AIY and AIA are the first-layer interneurons that receive synaptic inputs from ASEL (White, 1986, Fig. Intro4), but the role of each neuron for Na^+ chemotaxis had not been examined. AIB-ablated animals showed significantly reduced Na^+ chemotaxis when worms were cultivated at 100 mM Na^+ (Fig. 5a), suggesting that AIB is possibly required for transmission of sensory signals from ASEL. It is noteworthy that in the previous report NaCl chemotaxis was barely affected in AIB-ablated animals while klinokinesis was reduced (Kunitomo et al., 2013). On the other hand, chemotaxis of AIA- or AIY-ablated animals showed no significant difference from that of wild type (Fig. 5a). AIA/AIY double-ablated animals showed a defect in Na^+ chemotaxis (Fig. 5b), suggesting that AIA and AIY may redundantly act in ASEL-induced chemotaxis. It is also possible, however, that the observed Na^+ chemotaxis defect in AIY/AIA double mutant was caused by disabled locomotion ability (Fig. 5c), because both of the two interneurons are support forward locomotion (Fig. 8&9).

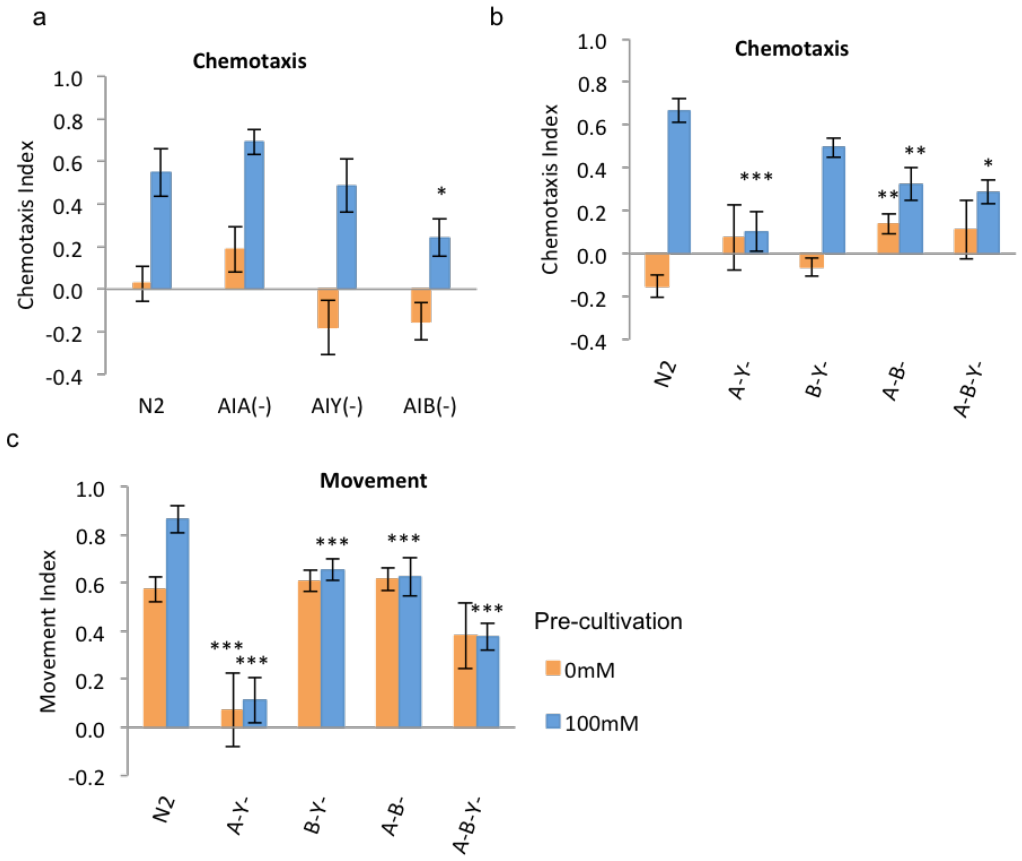

Figure 5 Na^+ chemotaxis of interneuron-ablated animals.

a, b, Na^+ chemotaxis of transgenic lines expressing mouse caspase in each class of interneurons or combinations of them (mean ± s.e.m, n ≥ 4, $p < 0.05$, $p < 0.01$, $p < 0.001$, *Dunnett's test*, significant difference between mutants and wild type). AIA (-): AIA-ablated strain; AIB (-): AIB-ablated strain; AIY (-): AIY-ablated strain; A-Y-: AIA- and AIY-ablated strain; A-B-: AIA- and AIB-ablated strain; B-Y-: AIB- and AIY-ablated strain; A-B-Y-: AIA-, AIB- and AIY-ablated strain. ***c,*** Movement index of animals in the same assay as (***b***). (*$p < 0.05$; ***$p < 0.001$, *Dunnett's test*, significant difference between mutants and wild type).

3.3 AIB, AIY and AIA are all required for the increase of forward locomotion generated by ASEL after cultivation with Na^+

3.3.1 AIB is required for forward locomotion by ASEL after cultivation with Na^+

AIB is activated upon downstep of NaCl concentrations depending on the off-response neuron ASER (Oda et al., 2011; Kunitomo et al., 2013). Because AIB was required for Na^+ chemotaxis, I investigated whether AIB is required for the behavioral response generated by ASEL activation of Na^+-cultivated animals. Suppression of turning induced by stimulation of ASEL was eliminated in AIB-ablated background irrespective of any Na^+ concentrations conditions (even without Na^+) (Fig. 6a, d&e). It was therefore suggested that AIB was required for stimulation of forward locomotion upon activation of ASEL by ChR2.

3.3.2 AIY is required for forward locomotion by ASEL after cultivation with Na^+

AIY is an important interneuron for controlling multiple behaviors and is involved in regulating reversal and gradual turning (Kocabas et al., 2012; Satoh et al., 2014). Behavioral responses induced by ASEL photoactivation were completely eliminated in AIY-ablated animals: there was no change in turning events both during and after activation of ASEL at any Na^+ concentration conditions (even without Na^+) (Fig. 6b, d&e).

3.3.3 AIA is required for forward locomotion by ASEL after cultivation with Na^+

AIA is activated in response to upsteps of NaCl concentrations, implying that AIA receives excitatory inputs from ASEL directly or indirectly (Oda et al., 2011). I found that ASEL-induced change of turning rates was significantly smaller or

eliminated in AIA-ablated animals (even without Na^+) (Fig. 6c-e), indicating that AIA is required for the behavioral response generated by ASEL. Thus, ASEL requires all first-layer interneurons, AIB, AIY, and AIA for generating the behavioral responses.

Figure is in the next page.

Figure 6 Interneurons are required for forward locomotion upon ASEL stimulation after cultivation with Na^+.

a-c, Behavioral response upon ASEL photoactivation of AIB-ablated animals (***a***), AIY-ablated animals (***b***) and AIA-ablated animals (***c***) Worms were transferred from 50 mM Na^+ cultivation to 100 mM Na^+ test condition (mean ± s.e.m, n ≥ 12). ***d,*** Change of turning event rate of interneuron-ablated animals in (***a-c***) during ASEL photoactivation (mean ± s.e.m) Difference between ATR (-) and ATR (+): $F_{(47, 550)} = 10.95$, $p < 0.0001$, $k = 24$, *kp < 0.05, **kp < 0.01, ***kp < 0.001, one way ANOVA followed by *t-test* with Bonferroni's correction. Difference of ATR (+) results between wild-type and ablation lines: ##p < 0.01, ###p < 0.001, *n. s.*, no significant difference, one way ANOVA followed by *Dennett's test*.

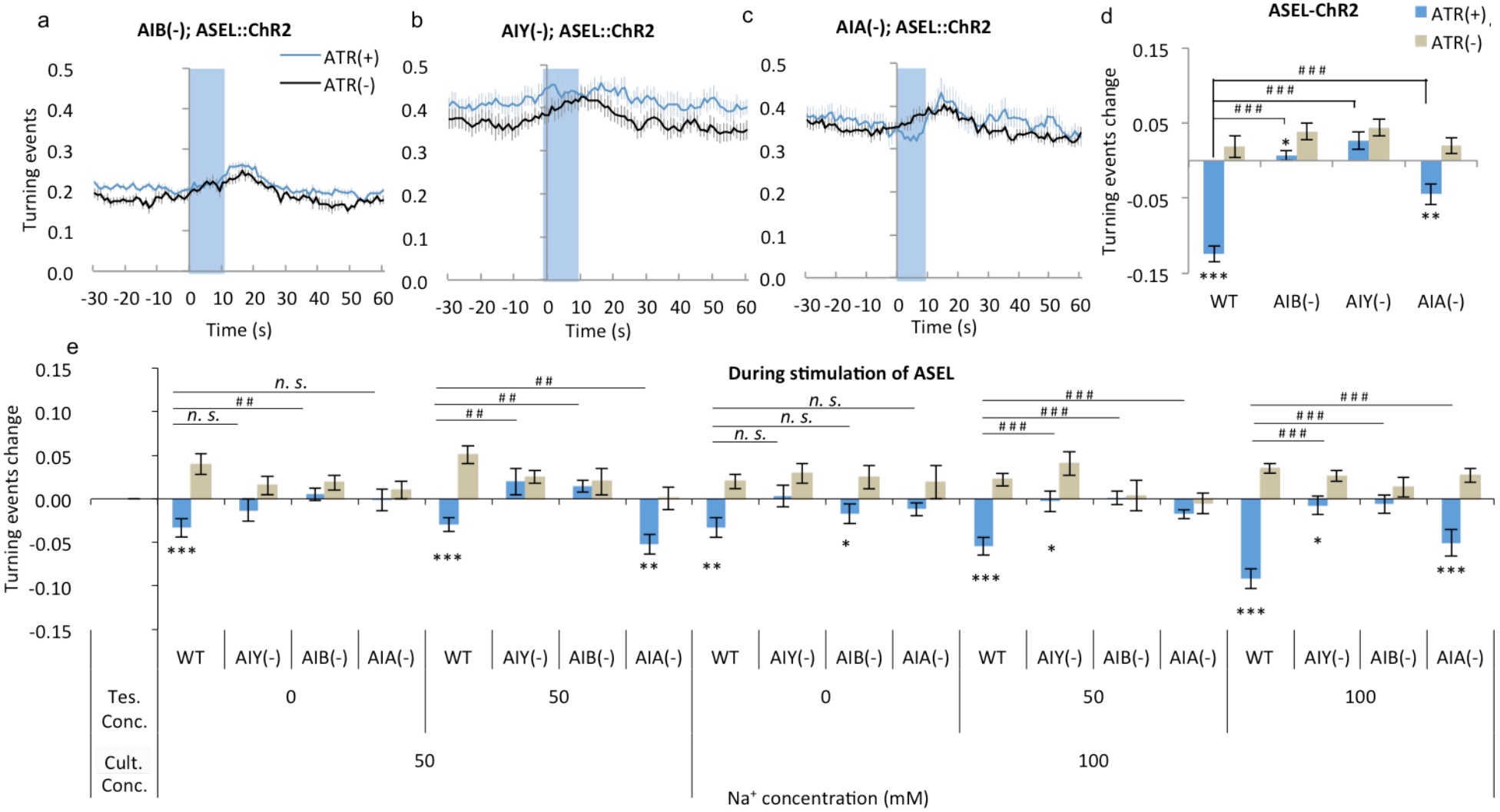
a
AIB(-); ASEL::ChR2
ATR(+)
ATR(-)
Turning events
Time (s)
b
AIY(-); ASEL::ChR2
Time (s)
c
AIA(-); ASEL::ChR2
Time (s)
d
ASEL-ChR2
ATR(+)
ATR(-)
Turning events change
WT
AIB(-)
AIY(-)
AIA(-)
e
During stimulation of ASEL
Turning events change
n. s.
WT
AIY(-)
AIB(-)
AIA(-)
Tes. Conc.
Cult. Conc.
0
50
100
Na⁺ concentration (mM)

3.4 AIB promotes turning behavior, whereas, AIY and AIA promotes forward locomotion

3.4.1 AIB promotes turning behavior

Interneurons AIB, AIY and AIA receive synaptic inputs from many sensory neurons including ASER, AWC, and ASEL, all of which are involved in chemotaxis to chemical cues (Chalasani et al., 2007, 2010; Kunitomo et al., 2013; Satoh et al., 2014). AIB respond to odor removal (Chalasani et al., 2007) or decreases in NaCl concentrations (Kunitomo et al., 2013), and stimulates turning behavior (Fig. Intro4). Behavioral assay showed that the rate of turning events increased during AIB stimulation by ChR2 under many conditions of Na^+ cultivated concentrations (Fig. 7).

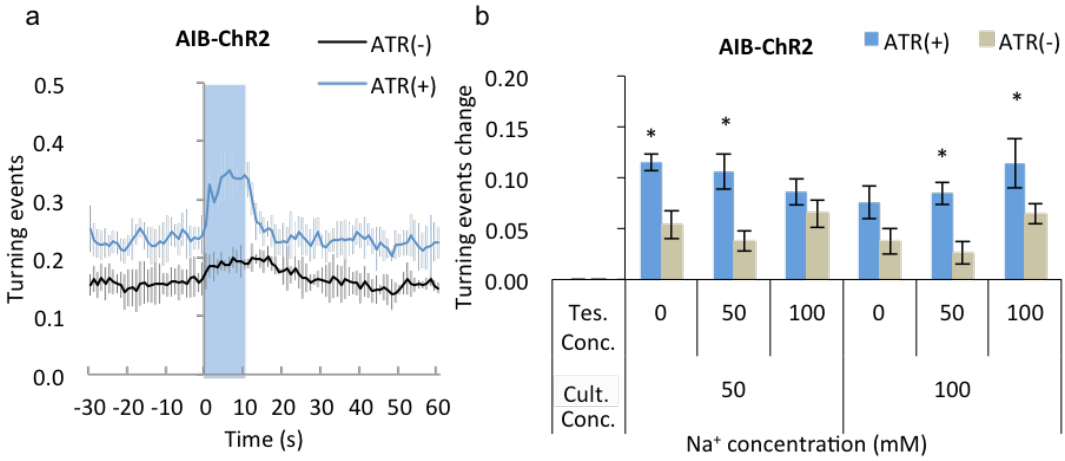

Figure 7 Worms' behavioral response induced by AIB photoactivation after cultivation with Na^+.

a, Worms' behavioral response when AIB was stimulated by ChR2 after worms were transferred from 50 mM Na^+ cultivation to 50 mM Na^+ test condition (mean±s.e.m, n≥12). ***b,*** Change of turning event rate upon photoactivation of AIB at different cultivation and test concentrations (mean ± s.e.m, n ≥ 12) Difference between ATR (-) and ATR (+): $F_{(11, 135)} = 5.046$, $p < 0.0001$; $k = 6$, *$kp < 0.05$, **$kp < 0.01$, ***$kp < 0.001$, one way ANOVA followed by *t-test* with Bonferroni's correction. For ATR (+) conditions: neither test concentrations ($F_{(2, 68)} = 0.08$, $p = 0.9194$) nor cultivation concentrations (F

$_{(1,\ 68)}$ = 0.67, p = 0.4146) have significant effect on behavioral response to AIB photostimulation, nor is there significant interaction between the two factors ($F_{(2,68)}$ = 2.84, p = 0.0654), two-way ANOVA.

3.4.2 AIY promotes forward locomotion

AIY was reported to show increased calcium level on odor addition and decreased calcium level on odor removal (Chalasani et al., 2007) and AIY activation promoted forward locomotion speed and inhibited turning (Fig. Intro4, Li et al., 2014). For stimulation of AIY, I utilized two strains that express ChR2 in AIY (strain#1 and #2). When AIY was stimulated by ChR2, in both strains, the ratio of turning events was decreased during AIY stimulation, and increased after stimulation under most cultivation conditions (Fig. 8).

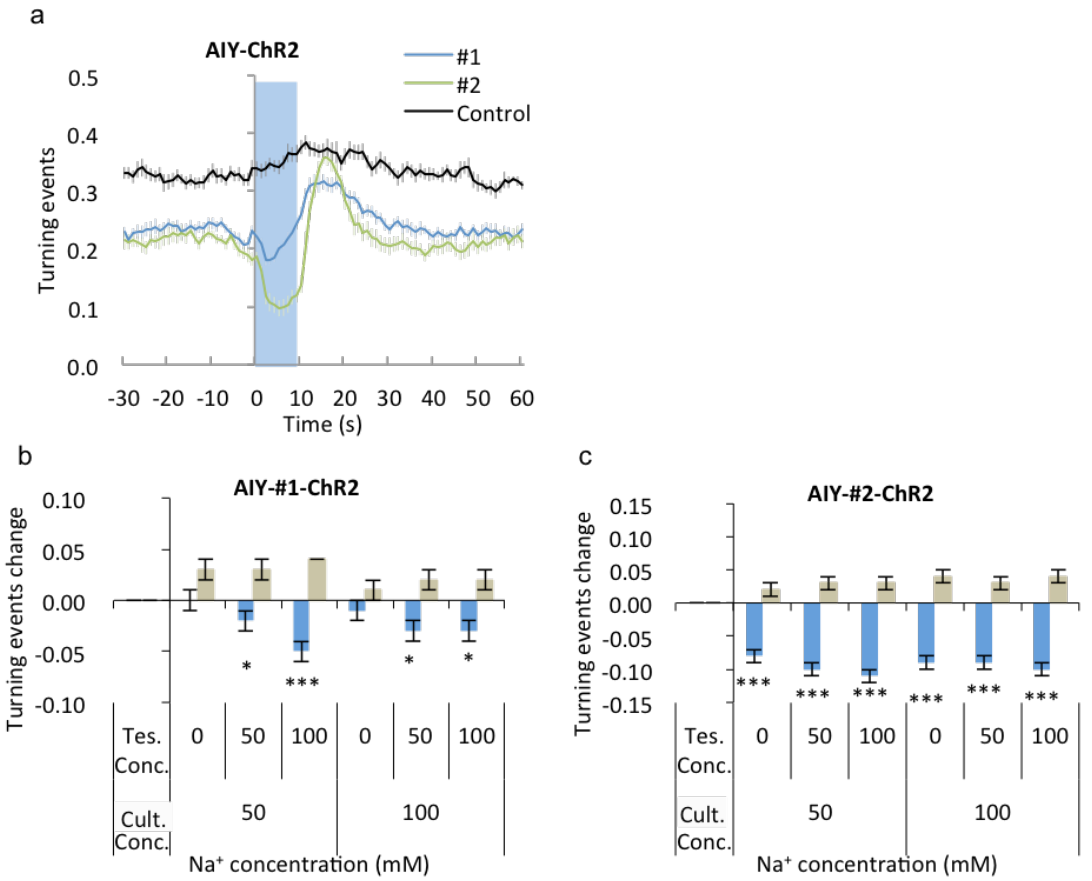

Figure 8 Worms' behavioral response to photoactivation of interneuron AIY after cultivation with Na^+.

a, Worms' behavioral response to AIY photostimulation. Worms were transferred from

50 mM Na^+ cultivation to 100 mM Na^+ test condition (mean ± s.e.m, n ≥ 12). ***b, c,*** Change of turning event rate upon photoactivation of AIY-#1 (***b***), AIY-#2 (See material and methods) (***c***), at different cultivation and test concentrations (mean±s.e.m, n≥12). Difference between ATR (-) and ATR (+): $F_{(11, 133)} = 9.365$, $p < 0.0001$ (***b***); $F_{(11, 131)} = 9.810$, $p < 0.0001$ (***c***); $k = 6$, $*kp < 0.05$, $**kp < 0.01$, $***kp < 0.001$, one way ANOVA followed by *t-test* with Bonferroni's correction. For ATR (+) conditions of AIY-#1-ChR2 (***b***): the test concentrations has significant effect on behavioral response to AIY photostimulation ($F_{(2, 67)} = 7.64$, $p = 0.0010$) while the cultivation concentrations has no significant effect ($F_{(1, 67)} = 0.08$, $p = 0.7830$) and there is no significant interaction between the two factors ($F_{(2, 67)} = 1.02$, $p = 0.3660$), two way ANOVA. For ATR (+) conditions of AIY-#2-ChR2 (***c***): neither test concentrations ($F_{(2, 67)} = 1.27$, $p = 0.2872$) nor cultivation concentrations ($F_{(1, 67)} = 0.00$, $p = 0.9508$) have significant effect on behavioral response to AIB photostimulation, nor is there significant interaction between the two factors ($F_{(2, 67)} = 0.45$, $p = 0.6364$), two-way ANOVA.

3.4.3 AIA promotes forward locomotion

It was reported that AIA is activated by addition of odor (Chalasani et al., 2010), and activated AIA inhibits turning behavior (Fig. Intro4, Larsch et al., 2015). Our result revealed that the behavioral response evoked by AIA stimulation was similar to that of AIY stimulation: the rate of turning events decreased during stimulation of AIA by ChR2 and increased after termination of AIA stimulation under all cultivated Na^+ conditions (Fig. 9). Thus, behavioral response to ASEL stimulation was similar to AIY or AIA stimulation but in contrast to AIB stimulation, suggesting a positive relationship between ASEL and AIY/AIA, but a negative relationship between ASEL and AIB.

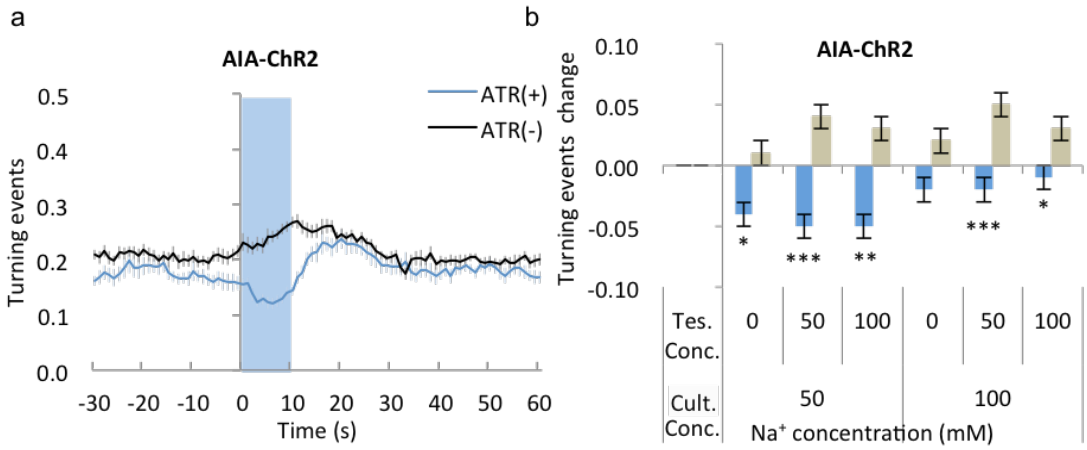

Figure 9 Worms' behavioral response to photoactivation of interneuron AIA after cultivation with Na^+.

a, Worms' behavioral response when AIA was stimulated by ChR2 after worms were transferred from 50 mM Na^+ cultivation to 100 mM Na^+ test condition (mean±s.e.m, n≥12). ***b,*** Change of turning event rate upon photoactivation of AIA at different cultivation and test concentrations (mean ± s.e.m, n ≥ 12) Difference between ATR (-) and ATR (+): $F_{(11, 141)} = 14.35$, $p < 0.0001$; $k = 6$, $*kp < 0.05$, $**kp < 0.01$, $***kp < 0.001$, one way ANOVA followed by *t-test* with Bonferroni's correction. For ATR (+) conditions: the cultivation concentrations have significant effect on behavioral response to AIA phtostimulation ($F_{(1, 65)} = 14.41$, $p = 0.0003$) while test concentrations has no significant effect ($F_{(2, 65)} = 0.36$, $p = 0.7002$) and there is no significant interaction between the two factors ($F_{(2, 65)} = 0.33$, $p = 0.7216$), two way ANOVA.

3.5 ASEL inhibits AIB and activates AIY and AIA after cultivation with Na^+

Next, we observed calcium responses of ASEL and the postsynaptic interneurons using RCaMP2 (Inoue et al., 2015) or RGECO (only for AIA) (Zhao et al., 2011) to directly observe the responses of each neuron during activation of ASEL.

3.5.1 Calcium response of ASEL upon ASEL photoactivation

3.5.1.1 ChR2-RGECO system

RFP-based GECIs, as a new color of GECIs, are expected to be combined with ChR2 for monitoring the neural activity induced by optogenetic stimlation using ChR2 (Zhang et al., 2011). The applicability of ChR2-RGECO system has been reported in a beta cell line and slice culture of developing mouse neocortex (Wu et al., 2013). Although unexpected nature of photoactivation phenomenon of RGECO by blue light had been reported, it could be avoided by using low intensity of blue-light illumination. Therefore, the applicability of ChR2-RGECO system expressed in ASEL neuron was investigated in this section.

3.5.1.1.1 RGECO probe apparently showed calcium response of ASEL to photoactivation after cultivation with Na^+ even without ATR

To simultaneously monitor the calcium responses of ASEL during optogenetic stimulation of the cell, ChR2 and RGECO were co-expressed in ASEL neuron (Fig. 10a). After cultivation with Na^+, RGECO florescence intensity was increased upon photo-activation of ASEL, and the intensity was correlated with the energy of illumination (Fig. 10b). Unexpectedly, this was the case also in conditions without ATR. Since opening of ChR2 strictly depend on the presence of ATR, light-induced RGECO fluorescence in the absence of ATR was not likely due to depolarization of ASEL but probably due to activation of the probe by blue light (Wu et al., 2013). However, there remains a possibility that coexpression of ChR2 and RGECO conferred blue light responsivity on the cell.

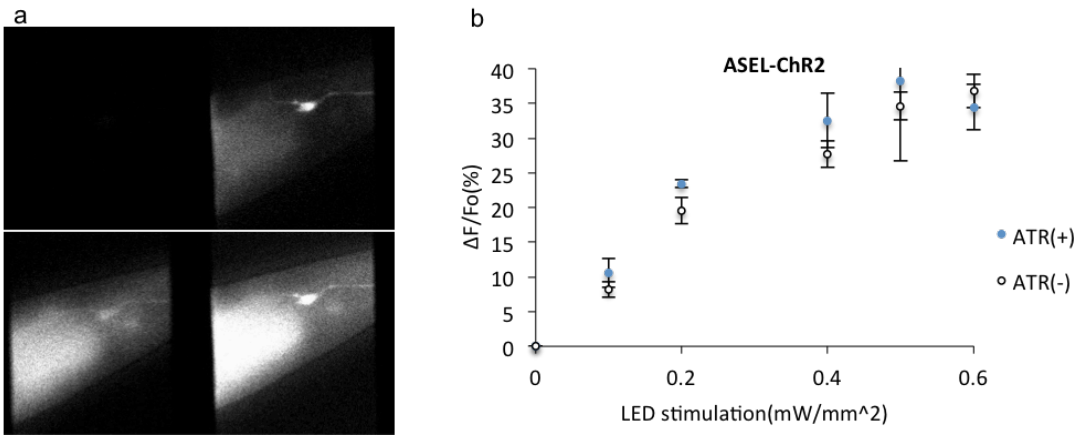

Fig. 10 Calcium response change of ASEL upon optical stimulation after cultivation with Na^+.

a, (top and bottom right) The RGECO fluorescence of ASEL under green light; (bottom left below) ChR2:: venus fluorescence of ASEL under blue light illumination. ***b,*** The calcium response of ASEL observed by using RGECO probe was positively related to optical stimulation strength, with no difference between ATR (+) and ATR (-) (mean ± s.e.m, n ≥ 12). Worms were illuminated at 50 mM Na^+ after cultivated at 50 mM Na^+.

3.5.1.1.2 The strain with ChR2-RGECO expression in ASEL had no behavioral defect

To test the possibility described above, we observed the behavioral response of this strain upon ChR2-mediated stimulation of ASEL. After cultivation with Na^+ and ATR, worms showed decreased turning events during ASEL stimulation and increased turning events after termination of ASEL stimulation, but no behavioral response under the condition of cultivation without ATR (Fig. 11a), indicated that ASEL was not stimulated in the absence of ATR, which was same as the strain that does not express RGECO probe (Fig. 11b). This result suggest that light induced RGECO fluorescence of ASEL in the strain does not reflect cell activity.

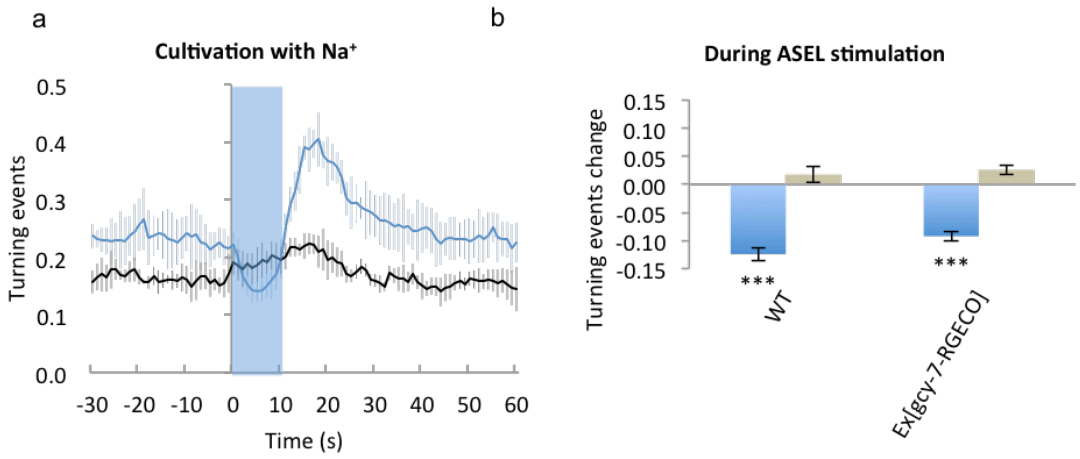

Fig. 11 Behavioral response to photoactivation of ASEL after cultivation with Na^+

a, Behavioral response of ASEL-RGECO-ChR2 strain upon ASEL photoactivation at 100 mM Na^+ after cultivation with 50 mM Na^+ (mean ± s.e.m, n ≥ 9). ***b,*** The change of turning events in (***a***) during stimulation of ASEL. The blue columns were under the conditions of cultivation with ATR, and the brown columns were under the conditions of cultivation without ATR.

3.5.1.1.3 RGECO probe expressed in ASEL showed autoactivation to blue light illumination.

The strain with expression of RGECO, but no ChR2 in ASEL, showed increased calcium response when NaCl concentration was increased (Fig. 12a), indicating RGECO probe could monitor calcium level accurately as GCaMP3 (See doctoral thesis of Dr. Hirofumi Sato). However, after cultivation with Na^+ without ATR, the fluorescence intensity of RGECO was positively correlated with the intensity of illumination by blue light (Fig. 12b), indicating that RGECO expressed in ASEL shows a photoactivation phenomenon, as described by Wu et al. (2013), which would disturb Ca^{2+} imaging traces during blue light illumination of ChR2.

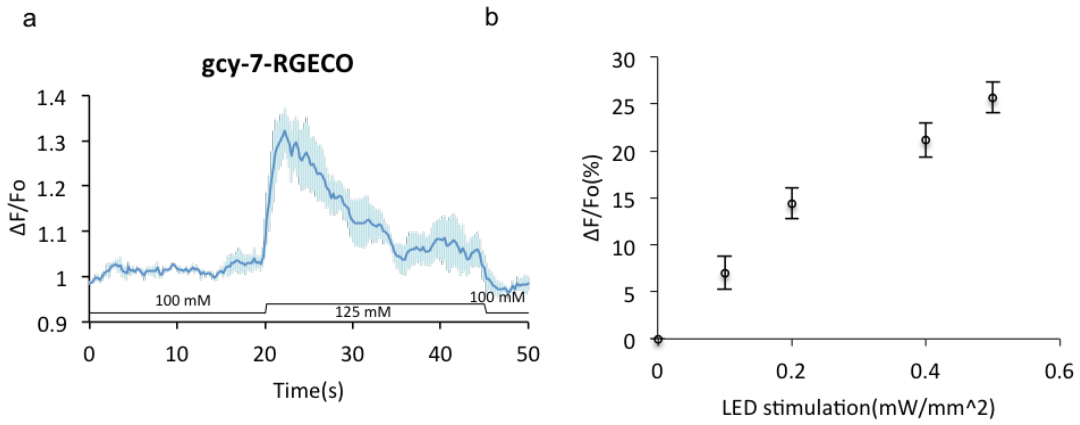

Fig. 12 Calcium response of ASEL with RGECO probe after cultivation with Na^+

a, Calcium response of ASEL-RGECO strain when NaCl concentration was changed from 100 mM at 20 s to 125 mM for 25 s and then back to 100 mM at 45 s after cultivation with Na^+ (mean ± s.e.m, n = 3). ***b,*** Calcium response change of ASEL-RGECO strain upon photo-stimulation after cultivation with Na^+ (mean ± s.e.m, n = 4). Worms were illuminated at 100 mM Na^+ after cultivation with 50 mM Na^+.

Thus, due to blue light-activation of RGECO probe expressed in ASEL concomitant use of ChR2 and RGECO is not suitable for observation of calcium response of ASEL upon photoactivation.

3.5.1.2 ChR2-RCaMP2 system

3.5.1.2.1 The transgenic line that express ChR2-RCaMP2 in ASEL showed no defect in the calcium response to salt concentration changes.

Animals that coexpress ChR2 and RCaMP2 probe in ASEL (Fig. 14a) showed increased calcium response when NaCl concentration was changed from 100mM to 125mM (Fig. 13), which is consistent with former reports (Suzuki et al., 2008; Doctoral thesis of Dr. Hirofumi Sato, 2016), indicating that this strain had no defect in the calcium response to salt concentration changes.

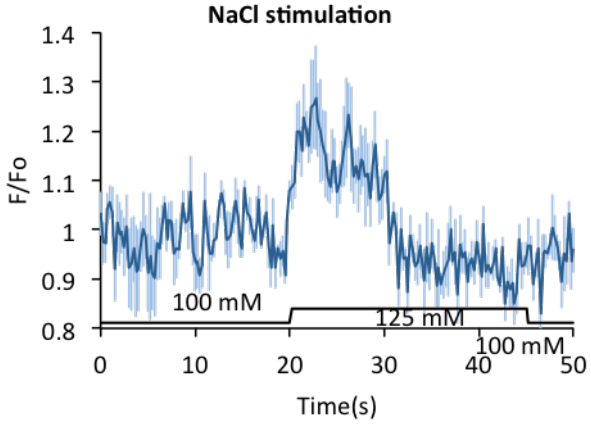

Fig. 13 Calcium response of ASEL with RCaMP2 probe and ChR2 in ASEL after cultivation with Na^+ (mean ± s.e.m, n = 3)

Worms were cultivated at 50 mM Na^+ and then subjected to calcium imaging in imaging buffer with 100 mM Na^+, which was further switched to 125 mM Na^+ after 20 s recording.

3.5.1.2.2 Calcium response of ASEL to photostimulation

After cultivation with Na^+ and ATR, the fluorescence intensity of RCaMP2 was was increased when ASEL was stimulated by blue light (Fig. 14b), whereas no response was observed in the absence of ATR (Fig. 22a), indicating that the activity of RCaMP2 reflects the activity of ASEL induced by photostimulation of ChR2.

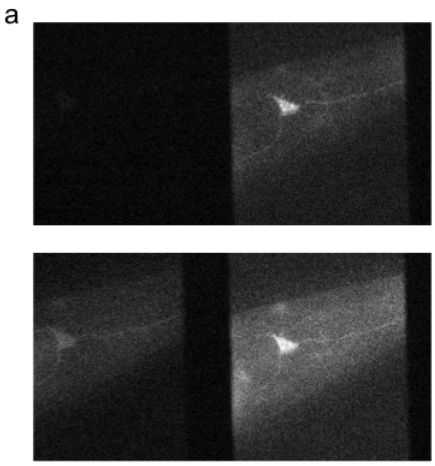

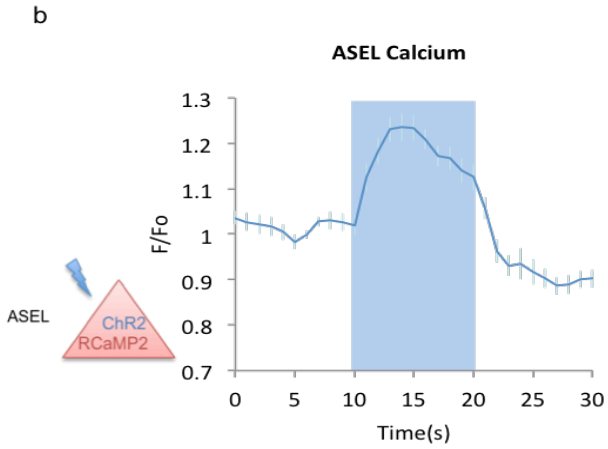

Fig. 14 Calcium response of ASEL to optical stimulation after cultivation with Na^+. ***a,*** (top and bottom right) The RCaMP2 fluorescence of ASEL under green light; (bottom left) ChR2::venus fluorescence of ASEL under blue light illumination. ***b,*** (left) Coexpression of ChR2 and RCaMP2 in ASEL; (right) Calcium response of ASEL upon ASEL photostimulation when worms were transferred from 50 mM Na^+ cultivation to 100 mM imaging buffer (See Material and Methods) (The optical stimulation strength was 0.5 mW/mm^2, mean ± s.e.m, n (ATR (+)) = 21, n (ATR (-)) = 18 (Fig. 22a)).

3.5.1.2.3 Calcium response change of ASEL is proportional to photoactivation strength.

Behavioral assay showed that the magnitude of worms' behavioral response increased upon stronger photostimulation of ASEL (Fig. 3b). The relationship between calcium response of ASEL and the strength of photostimulation was investigated under the conditions of cultivation with Na^+. The results showed that when worms were cultivated with Na^+ and ATR, the calcium level change of ASEL was proportional to the intensity of illumination in the range of 0~0.5 mW/mm^2 (Fig. 15). It is indicated that ASEL's activity is linearly related to the strength of photoactivation of the cell in the range of 0~0.5 mW/mm^2.

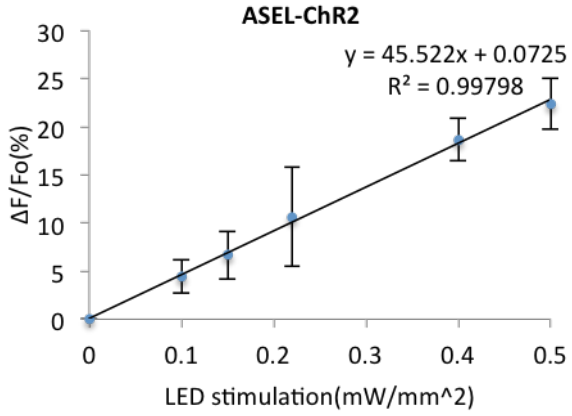

Fig. 15 Calcium response of ASEL to photoactivation in different strengths after cultivation with Na^+ (mean ± s.e.m, n = 3)

Worms were cultivated at 50 mM Na^+ and then illuminated at 100 mM Na^+.

3.5.2 Calcium response of AIB upon ASEL activation

3.5.2.1 Calcium response of AIB to NaCl stimulation in the strain with expression of ChR2 in ASEL

RCaMP2 probe was used to observe calcium response of AIB, and the result showed that calcium level of AIB with RCaMP2 indicator was increased when NaCl concentration was decreased from 25mM to 0mM, and then decreased to the basal level when NaCl concentration was returned to 25mM (Fig. 16). This was consistent with the calcium response of AIB using GCaMP indicator (See doctoral thesis of Dr. Hirofumi Sato), indicating that the strain that expresses RCaMP2 in AIB and ChR2 in ASEL showed no defect in the calcium response of AIB to salt concentration changes.

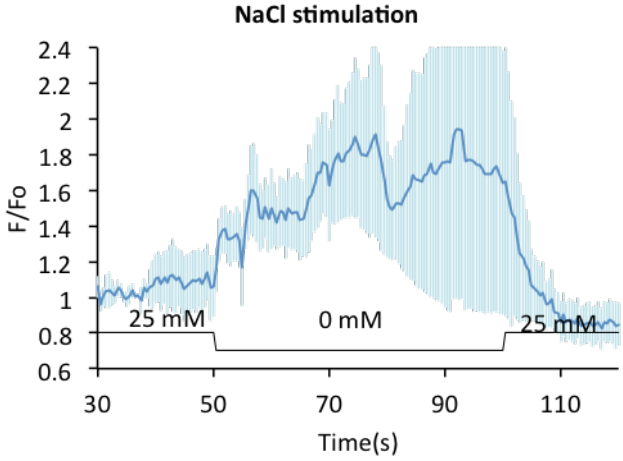

Fig. 16 Calcium response of AIB to NaCl stimulation in the strain with ChR2 expression in ASEL after cultivation with Na^+ (mean ± s.e.m, n = 3)

After cultivation at 50 mM NaCl, worms were placed in imaging buffer with 25 mM NaCl and recorded for 50 s and changed to 0 mM NaCl imaging buffer for 50 s, then shifted back to 25 mM NaCl imaging buffer.

3.5.2.2 Calcium response of AIB cell body to ASEL photoactivation after cultivation with Na^+

Using above verified strain that express RCaMP2 in AIB and ChR2 in ASEL, calcium responses of AIB to ASEL photoactivation was observed in this section The results indicated that the calcium level of AIB cell body decreased upon ASEL photo-stimulation (Fig. 17a), indicating that AIB was inhibited by ASEL activation. Besides, calcium change of AIB was prominent when the blue light strength was increased to 0.5 mW/mm^2, suggesting that AIB was effectively inhibited by ASEL under strong photoactivation.

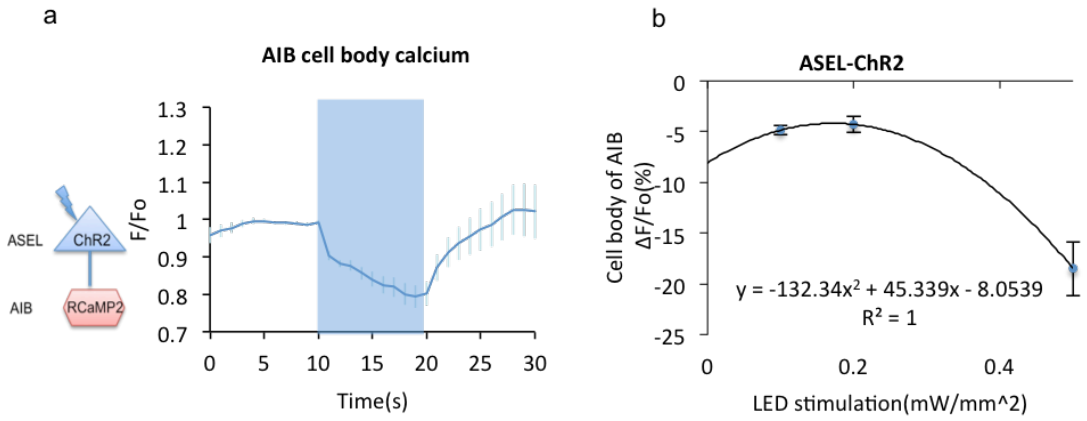

Fig. 17 Calcium response of AIB cell body to ASEL photoactivation after cultivation with Na^+

a, (left) A schematic of AIB expression of RCaMP2 in transgenic worms in which ChR2 was expressed in ASEL; (right) Calcium response of AIB cell body upon ASEL photostimulation when worms were transferred from 50 mM Na^+ cultivation to 100 mM imaging buffer (The Optical stimulation strength was 0.5 mW/mm^2, mean±s.e.m, n (ATR (+)) = 22; n (ATR (-)) = 19). ***b,*** Calcium response of AIB to ASEL photoactivation in different strengths of stimuli after cultivation with 50 mM Na^+ (mean ± s.e.m, n ≥ 10)

3.5.2.3 Calcium response of AIB process to ASEL photoactivation after cultivation with Na^+

Similar to calcium response of AIB cell body, the calcium level of AIB process was decreased significantly upon ASEL photostimulation (Fig. 18a, 22a), indicating that AIB was inhibited by ASEL. Besides, calcium change of AIB was increased sharply when the blue light strength was increased to 0.5 mW/mm^2, suggesting that AIB received effective signal from ASEL and was inhibited by ASEL only with strong photoactivation.

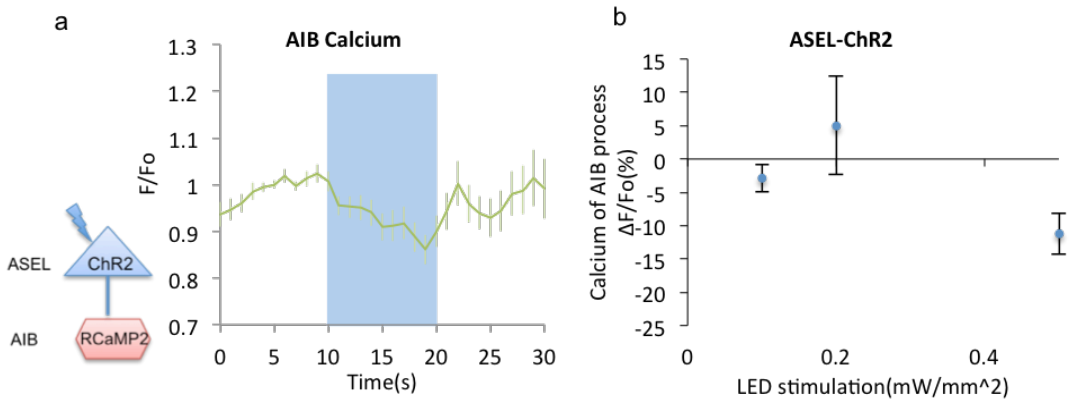

Fig. 18 Calcium response of AIB process to ASEL photoactivation after cultivation with Na^+

a, (left) A schematic of AIB expression of RCaMP2 in transgenic worms in which ChR2 was expressed in ASEL; (right) Calcium response of AIB process upon ASEL photo-stimulation when worms were transferred from 50 mM Na^+ cultivation to 100 mM imaging buffer (The optical stimulation strength was 0.5 mW/mm^2, mean ± s.e.m, n (ATR (+)) = 22; n (ATR (-)) = 19 (Fig. 22a)). ***b,*** Calcium response of AIB process to ASEL photoactivation in different strengths after cultivation with 50 mM Na^+ (mean ± s.e.m, n ≥ 10)

Thus, the calcium level of AIB was decreased upon ASEL activation under the conditions of cultivation with Na^+. As inhibition of AIB suppress turning, afore mentioned behavior evoked by ASEL photoactivation might be mediated by AIB.

3.5.3 Calcium response of AIY upon ASEL photoactivation

AIY's calcium content was increased during photoactivation of ASEL, revealing that AIY was activated by ASEL (Fig. 19a, 22a). Besides, unlike AIB, AIY was activated upon ASEL photoactivation within a low strength (0.1 mW/mm^2), and the calcium change of AIY reached to peak in the strength of 0.15 mW/mm^2, kept to plateau until 0.4 mW/mm^2, and decreased in the strength of 0.5 mW/mm^2 (Fig. 19b). It is suggested that AIY showed a sensitive range of stimulation, which is different from that of AIB, whose calcium response was increased along with stimulus intensity (Fig. 18b).

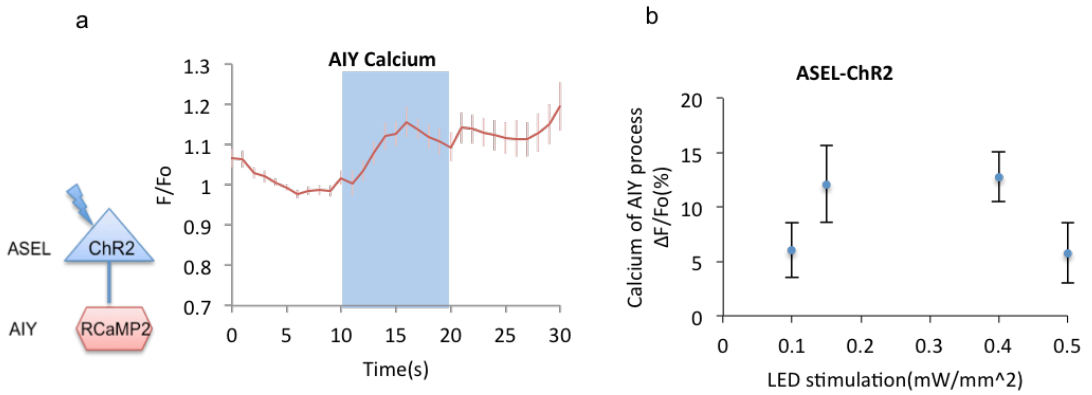

Fig. 19 Calcium response of AIY process to ASEL photo-activation after cultivation with Na^+

a, (left) A schematic of AIY expression of RCaMP2 in transgenic worms in which ChR2 was expressed in ASEL. (right) AIY calcium response when ASEL was stimulated by ChR2 when worms were transferred from 50 mM Na^+ cultivation to 100 mM imaging buffer (The optical stimulation strength was 0.4 mW/mm^2, mean ± s.e.m, n (ATR (+)) = 23; n (ATR (-)) = 22 (Fig. 22a)). ***b,*** Calcium response of AIY process to ASEL photoactivation in different strengths after cultivation with Na^+ (mean ± s.e.m, n ≥ 10)

3.5.4 Calcium response of AIA upon ASEL photoactivation

3.5.4.1 Calcium response of AIA cell body to ASEL photoactivation after cultivation with Na^+

The results showed that AIA cell body showed no obvious calcium response upon ASEL photo-stimulation in the stimulus range up to 0.5 mW/mm^2 (Fig. 20), which is consistent with the previous report that AIA cell body showed no calcium response upon NaCl concentration changes (Oda et al., 2011).

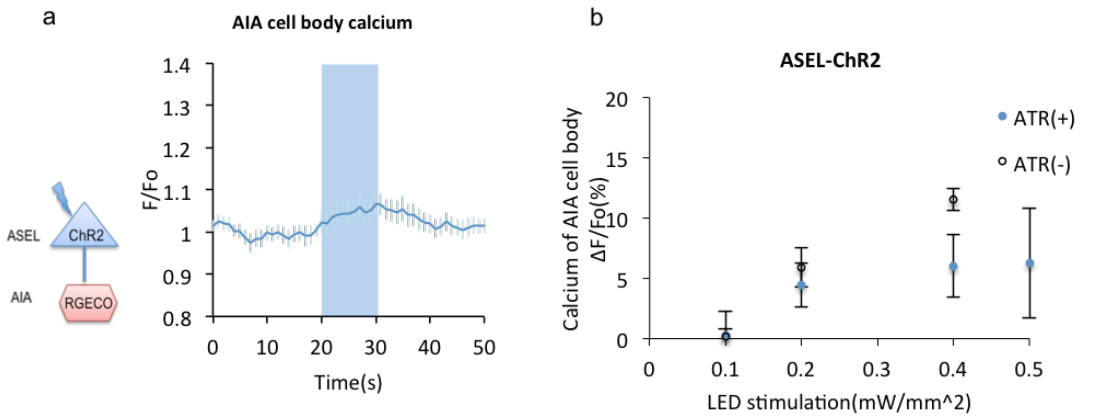

Fig. 20 Calcium response of AIA cell body to ASEL photoactivation after cultivation with Na^+

a, (left) A schematic of AIA expression of RGECO in transgenic worms in which ChR2 was expressed in ASEL. (right) AIA cell body calcium response during ASEL stimulation by ChR2 when worms were transferred from 50 mM Na^+ cultivation to 100 mM imaging buffer (The optical stimulation strength was 0.5 mW/mm^2, mean ± s.e.m, n (ATR (+)) = 11; n (ATR (-)) = 16). ***b,*** Calcium response of AIA cell body to ASEL photoactivation in different strengths after cultivation with 50 mM Na^+ (mean ± s.e.m, n ≥ 10).

3.5.4.2 Calcium response of AIA process to ASEL photoactivation after cultivation with Na^+

Similar to AIY, calcium response of AIA process was increased upon ASEL stimulation, indicating that AIA was also activated by ASEL (Fig. 21a, 22a). Similar to ASEL, calcium change of AIA increased linearly along with the intensity of photo-activation in the range of 0~0.4 mW/mm^2 (Fig. 21b), indicating that calcium response change of AIA is linearly related to the blue light photoactivation of ASEL.

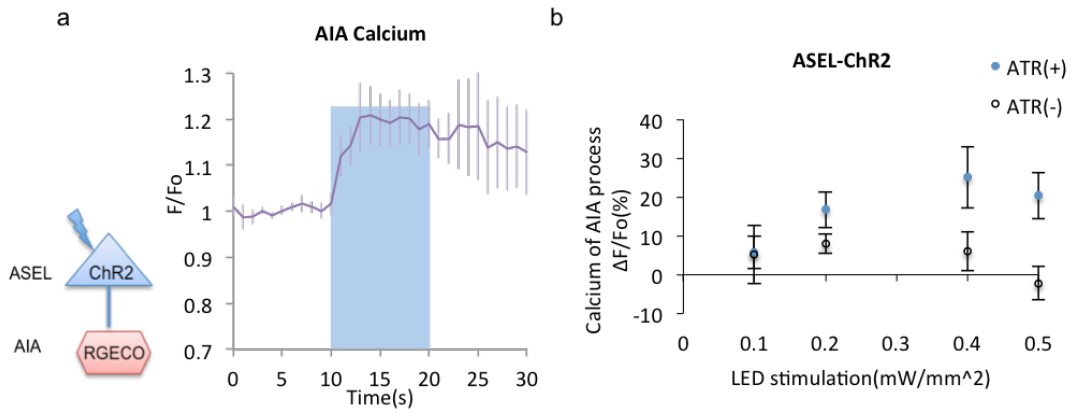

Fig. 21 Calcium response of AIA process to ASEL photoactivation after cultivation with Na^+

a, (left) A schematic of AIA expression of RGECO in transgenic worms in which ChR2 was expressed in ASEL. (right) AIA process calcium response during ASEL stimulation by ChR2 when worms were transferred from 50 mM Na^+ cultivation to 100 mM imaging buffer (The optical stimulation strength was 0.5 mW/mm^2, mean ± s.e.m, n (ATR (+)) = 11; n (ATR (-)) = 16). ***b,*** Calcium response of AIA process to ASEL photoactivation in different strengths after cultivation with 50 mM Na^+ (mean ± s.e.m, n ≥ 10)

3.3~5 Conclusion

All three first-layer interneurons respond to activation of ASEL: AIB was inhibited by ASEL, while AIY and AIA were activated by ASEL (Fig. 22a). All of these transmissions promote forward locomotion, and therefore all three interneurons may contribute to driving worms to higher Na^+ concentrations (Fig. 22b). Furthermore, AIY was activated in a low range of photoactivation strength of ASEL; activity of AIA was linearly related to the photoactivation strength of ASEL, which was similar to the activation pattern to ASEL; AIB was inhibited obviously at high photoactivation strength of ASEL.

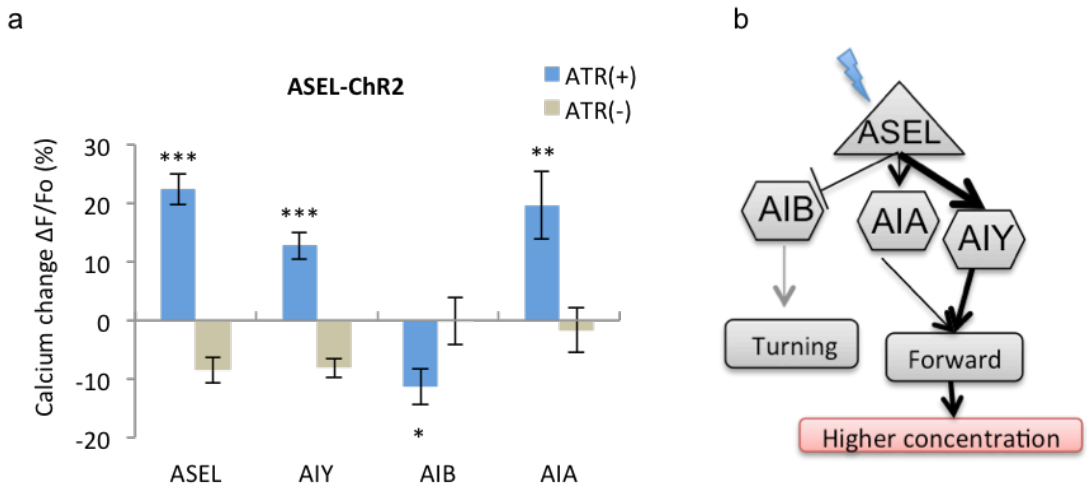

Fig. 22 Calcium response of interneurons to ASEL photoactivation after cultivation with Na^+

a, Calcium response change of neurons (***m-p***) during stimulation of ASEL. Difference between ATR (-) and ATR (+): $F_{(7, 137)} = 17.84$, $p < 0.0001$, $k = 4$, $^*kp < 0.05$, $^{**}kp < 0.01$, $^{***}kp < 0.001$, one way ANOVA followed by *t-test* with Bonferroni's correction. ***b,*** A speculated diagram for neural circuit downstream of ASEL after cultivation with 50 mM Na^+.

3.6 Cellular basis of the behavioral plasticity caused by cultivation with/without Na^+

3.6.1 Behavioral plasticity caused by cultivation without Na^+

In the chemotaxis assay, I observed that when worms were cultivated in NaCl-free conditions, worms had no Na^+ concentration preference (Fig. 1). We therefore tested the behavioral response to ASEL stimulation after NaCl-free cultivation. When worms were cultivated in NaCl-free conditions, they showed no behavioral response to ASEL photostimulation in Na^+-containing conditions (Fig. 23).

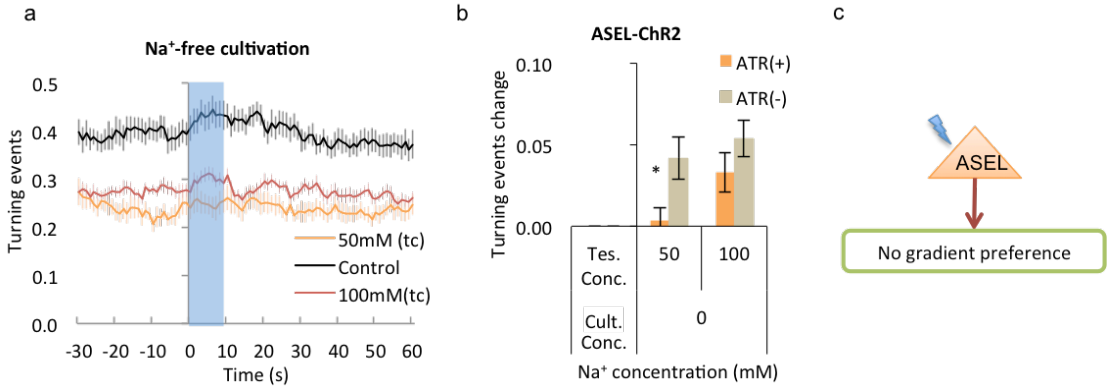

Fig. 23 Behavioral response of worms upon ASEL photoactivation after cultivation without Na^+

a, Behavioral response to optical stimulation of ASEL when worms were transferred from Na^+-free cultivation to 50 mM Na^+ (black line (NO ATR) and orange line (with ATR)) and 100 mM Na^+ (with ATR) (mean±s.e.m, n≥12). ***b,*** Change of turning event rate in (***a***). Difference between ATR (-) and ATR (+): $F_{(3, 47)} = 3.31$, $p = 0.0278$, $k = 2$, $*kp < 0.05$, one way ANOVA followed by *t-test* with Bonferroni's correction. ***c,*** A schematic of worms' behavioral response generated by ASEL after Na^+-free cultivation.

3.6.2 Na^+ but not Cl^- is important for NaCl-dependent behavioral plasticity

I tested which ion, Na^+ or Cl^-, when present during pre-assay cultivation, contributes to the behavioral response to ASEL stimulation. NaCl was replaced by NaAc for either cultivation or test plates. As a result, worms showed similar behavioral response upon ASEL's activation after NaCl or NaAc cultivation (Fig. 24a): they showed increased forward movement during stimulation and increased turning after termination of photostimulation of ASEL. Likewise, replacing NaCl with NaAc in test plates did not cause significant difference (Fig. 24), indicating that Na^+ is responsible for the plasticity in the behavioral response to ASEL stimulation.

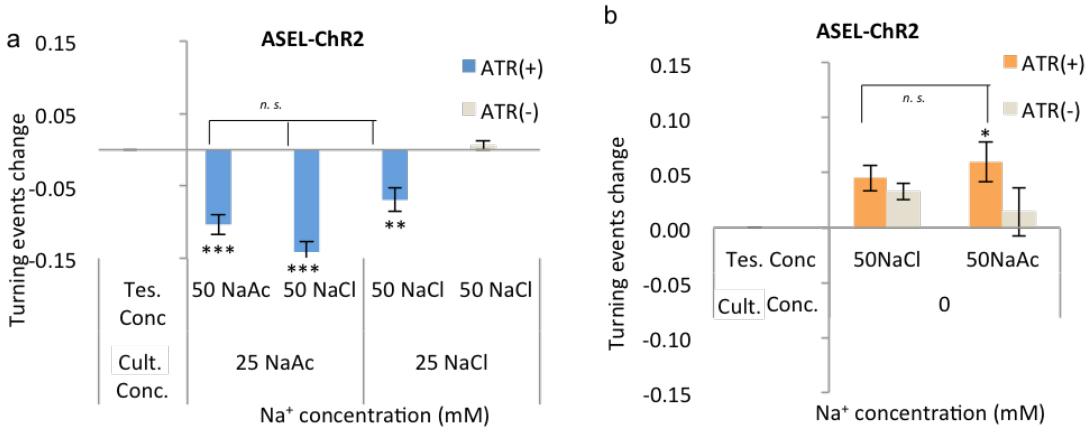

Fig. 24 Worms' behavioral response to ASEL photoactivation under NaCl and NaAc conditions.

a, Change of turning event rate during ASEL stimulation for 60 s when worms were transferred from NaAc or NaCl cultivation to test concentrations of NaAc or NaCl (mean ± s.e.m, n ≥ 6). Difference between ATR (-) and ATR (+): $F_{(3, 22)} = 13.08$, $p < 0.0001$; *$p <$ 0.05, ***p < 0.001, *n. s.,* no significant difference, one way ANOVA followed by Bonferroni's multiple comparison. ***b,*** Change of turning event rate during ASEL stimulation for 60 s when worms were transferred from Na^+-free cultivation to test concentrations with NaAc or NaCl (mean ± s.e.m, n ≥ 6). Difference between ATR (-) and ATR (+): $F_{(3, 49)} = 1.36$, $p = 0.2661$, $k = 2$, *n. s.,* no significant difference, one way ANOVA followed by *t-test* with Bonferroni's correction.

3.6.3 Stimulation of ASEL generates Na^+-dependent behavioral plasticity.

The next question was whether Na^+ is directly sensed by ASEL during pre-assay cultivation to generate behavioral plasticity. To answer this question, I made use of the *dyf*-11 mutant, which has deformed cilia and therefore cannot sense water-soluble chemicals (Kunitomo and Iino, 2008). When worms were cultivated with Na^+, reduction of turning was not observed in *dyf-11* mutant when ASEL was stimulated by ChR2, and this defect was rescued by *dyf-11* expression only in ASEL (Fig. 25a&b). When worms were cultivated in Na^+-free conditions, increase in turning events upon ASEL photoactivation was observed in the *dyf-11* mutant, and this response was suppressed by *dyf-11* expression in ASEL neuron (Fig. 25c&d). These results indicated that ASEL generates Na^+-dependent plasticity (behavioral response only after cultivation with Na^+).

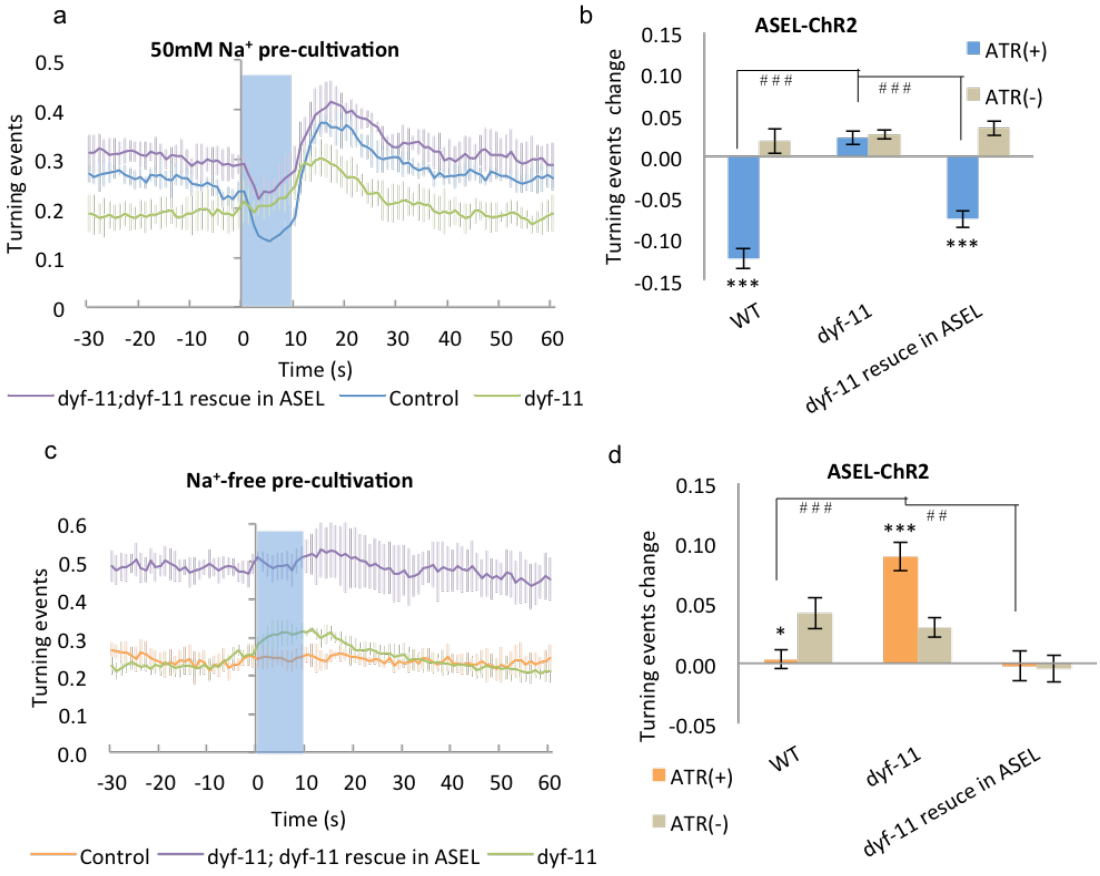

Fig. 25 Bavioral response of *dyf-11* mutants to ASEL photoactivation after cultivation with/without Na^+.

a, Behavioral response of wild type, *dyf-11* mutant and rescued animals whose ASEL was solely rescued to ASEL photostimulation at 50 mM Na^+ after Na^+-free cultivation (mean ± s.e.m, n ≥ 12). ***b,*** Change of turning event rate in (***a***) Difference between ATR (-) and ATR (+): $k = 3$, ***$kp < 0.001$; Difference between *dyf-11* and other strains: ###$p < 0.001$, $F_{(5, 70)} = 44.25$, $p < 0.0001$, one way ANOVA followed by Bonferroni's multiple comparison. ***c,*** Behavioral response of *dyf-11* mutants to ASEL photostimulation at 100 mM Na^+ after cultivation at 50 mM Na^+ (mean ± s.e.m, n ≥ 12). ***d,*** Change of turning event rate in (***c***). Difference between ATR (-) and ATR (+): **$p < 0.01$; Difference between *dyf-11* and other strains: ###$p < 0.001$, $F_{(5, 64)} = 10.70$, $p < 0.0001$, one way ANOVA followed by Bonferroni's multiple comparison.

3.6.4 Na^+-dependent behavioral plasticity is not observed upon photostimulation of downstream interneurons.

Upon ASEL stimulation, behavioral plasticity was observed in different cultivations conditions, cultivation with/without Na^+. To dissect the neural circuits that generate Na^+ plasticity, the role of first layer interneurons was investigated. AIB, AIY or AIA was stimulated by ChR2 in wild-type background. Animals showed similar responses both under Na^+-free and Na^+-present conditions(Figs. 7-9, 26). This implied that the difference in the behavioral responses after Na^+-containing and Na^+-free cultivation was attributed to neuronal responses upstream of first-layer interneurons, possibly in ASEL.

Figure is in the next page.

Fig. 26 Bavioral response of worms to interneurons photoactivation after cultivation without Na^+.

a-c, Behavioral response upon photoactivation of AIB (***a***), AIY (***b***) or AIA (***c***) when worms were transferred to 50 mM Na^+ after Na^+-free cultivation (mean ± s.e.m, n ≥ 11). ***d-g,*** Change of turning event rate during stimulation of AIB (***d***), AIY-#1 (***e***), AIY-#2(***f***), or AIA (***g***) when worms were transferred to different Na^+ concentrations after Na^+-free cultivation. Difference between ATR (-) and ATR (+): (***b***) $F_{(3, 44)} = 15.47$, $p < 0.0001$, $k = 2$,

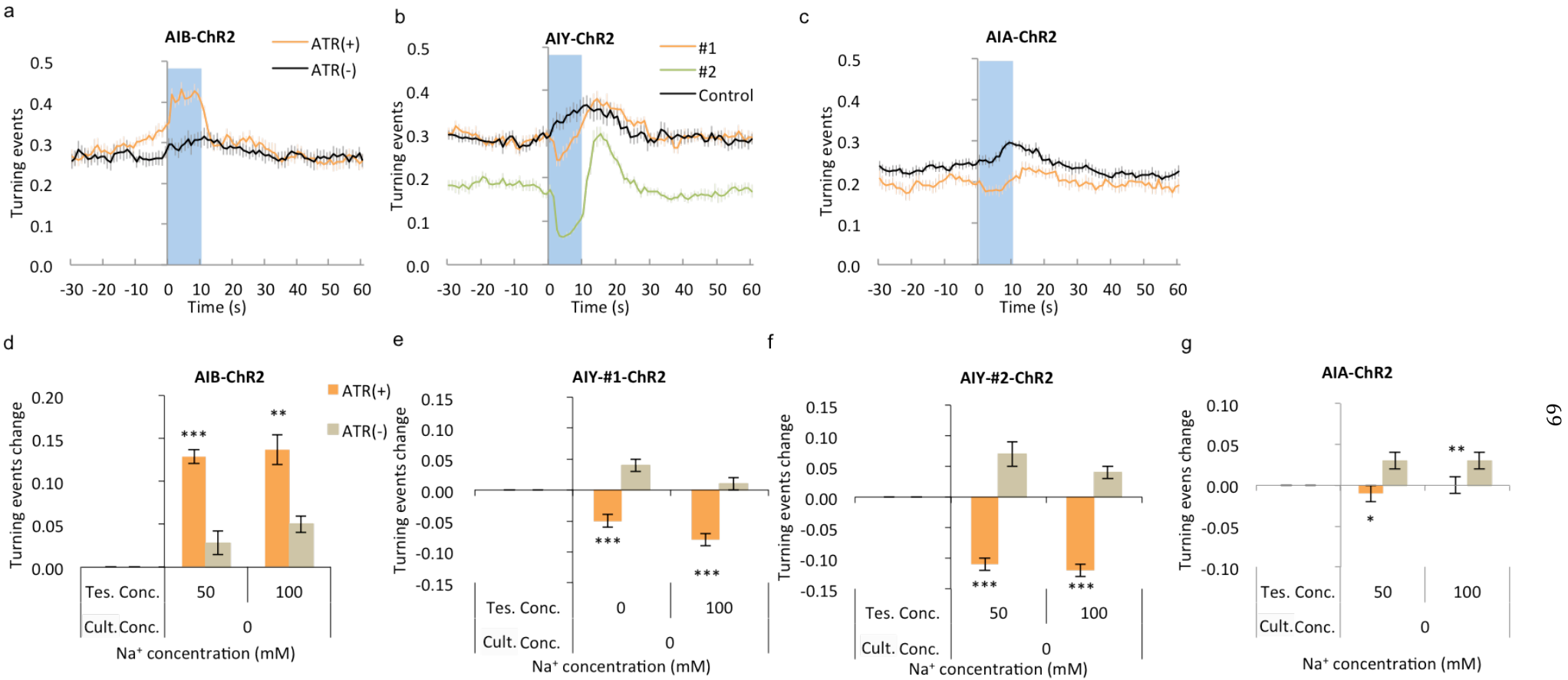
a
AIB-ChR2
ATR(+)
ATR(-)
Turning events
Time (s)
b
AIY-ChR2
#1
#2
Control
Turning events
Time (s)
c
AIA-ChR2
Turning events
Time (s)
d
AIB-ChR2
ATR(+)
ATR(-)
Turning events change
Tes. Conc.
Cult. Conc.
Na⁺ concentration (mM)
e
AIY-#1-ChR2
Turning events change
Tes. Conc.
Cult. Conc.
Na⁺ concentration (mM)
f
AIY-#2-ChR2
Turning events change
Tes. Conc.
Cult. Conc.
Na⁺ concentration (mM)
g
AIA-ChR2
Turning evens change
Tes. Conc.
Cult. Conc.
Na⁺ concentration (mM)

kp < 0.0001; (c***) $F_{(3,43)}$ = 71.67, p < 0.0001; (***d***) $F_{(3,42)}$ = 6.88, p = 0.0007, k = 2, *kp < 0.05, ***kp < 0.001; (***e***) $F_{(3,45)}$ = 29.06, p < 0.001, k = 2, ***kp < 0.001; k = 2, ***kp < 0.001, one way ANOVA followed by *t-test* with Bonferroni's correction.

3.6.5 The sensory neuron ASEL is responsible for Na^+ behavioral plasticity.

Since Na^+-dependent behavioral plasticity was not observed if first layer interneurons were directly activated (Fig. 26), it is possible that Na+ plasticity is caused by a synaptic change between ASEL and first layer interneurons, and it is also possible that Na+ plasticity is caused by the sensory neuron ASEL. ASEL showed no calcium response upon ASEL photostimulation after Na^+-free cultivation (Fig. 27), suggesting that Na+ plasticity is possibly caused by a change in the intrinsic excitability of ASEL neuron, but not the connectivity change between ASEL and first layer interneurons. This is likely the reason why there was no behavioral response to ASEL stimulation after Na^+-free cultivation, and no Na^+ concentration preference after cultivation in Na^+-free conditions (Fig. 23c).

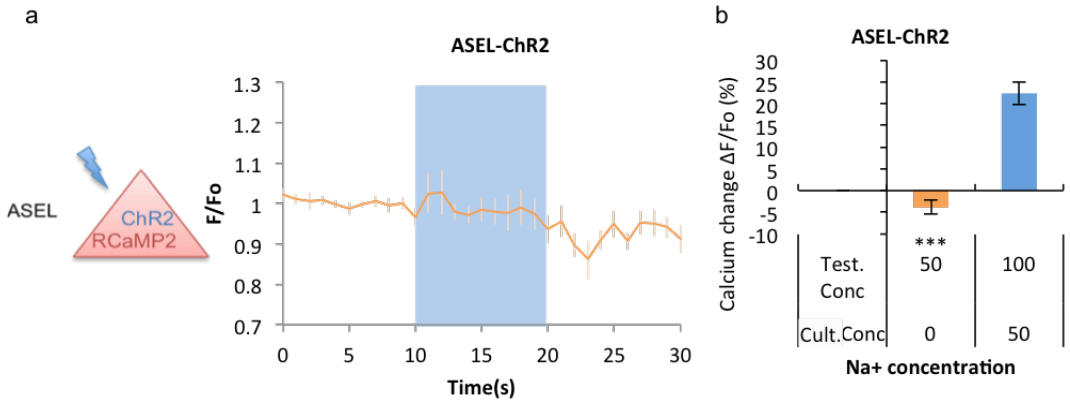

Fig. 27 Calcium response of ASEL to optical stimulation after cultivation without Na^+

a, (left) Coexpression of ChR2 and RCaMP2 in ASEL; (right) Calcium response of ASEL upon ASEL photostimulation in 50 mM imaging buffer after Na^+-free cultivations (The optical stimulation strength was 0.5 mW/mm^2, mean ± s.e.m, n (ATR (+)) = 22; n (ATR (-)) = 20). ***b,*** Calcium response change of ASEL neuron(***Fig.27a & Fig. 14b***) during

stimulation of ASEL (***$p < 0.001$, student *t-test*).

3.7 *eat-4* and *egl-30* in ASEL are involved in ASEL-triggered behavioral response

3.7.1 *eat-4* in ASEL is involved in ASEL-triggered behavioral response

eat-4, which encodes a vesicular glutamate transporter, is necessary for glutamatergic transmission in *C. elegans* (Lee et al., 1999; Rand et al., 2000). *eat-4* is also expressed in ASE neurons (Serrano-Saiz et al., 2013), which implies that ASE neurons release glutamate onto downstream interneurons. An *eat-4* mutation eliminated the behavioral response upon ASEL activation after cultivation with Na^+. Moreover, cell-specific knockdown of *eat-4* in ASEL by RNA interference caused smaller behavioral responses than those in wild type during ASEL stimulation (Fig. 28), suggesting that glutamate is used as a neurotransmitter in ASEL for the behavioral responses.

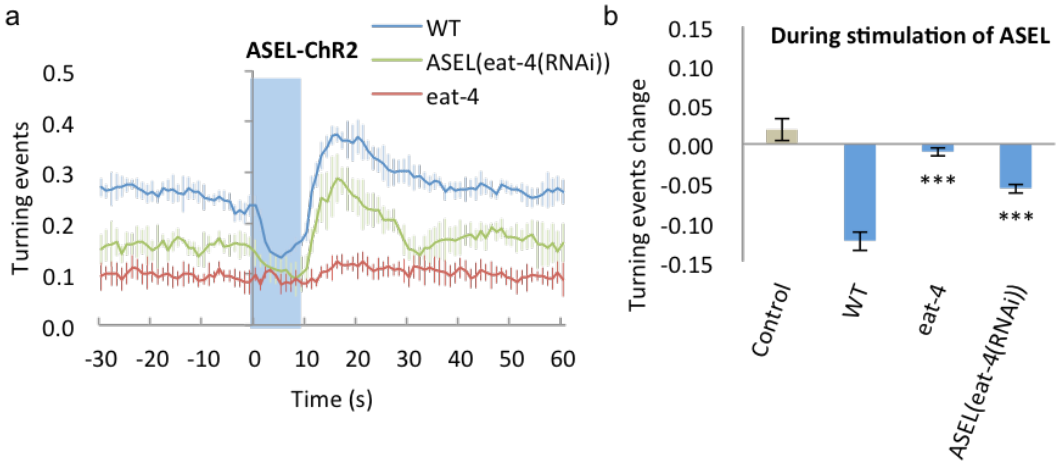

Fig. 28 Behavioral response of *eat-4* mutants to ASEL photoactivation.

a, Behavioral response of *eat-4* mutants upon ASEL photoactivation at 100 mM Na^+ after 50 mM Na^+ cultivation (mean ± s.e.m, n ≥ 7). ***b,*** Change of turning event rate in (***a***). Difference between wild type and mutants: ***$p < 0.001$, one way ANOVA followed by *Dunnett's-test*.

3.7.2 *egl-30* in ASEL is involved in ASEL-triggered behavioral plasticity

egl-30, which encodes an ortholog of the alpha subunit of heterotrimetric G-protein Gq, positively regulates locomotory movements (Brundage et al., 1996; Lackner et al., 1999; Adachi et al., 2010). The Gq/DAG/PKC pathway modulates NaCl chemotaxis and counteracts the phosphatidylinositol 3-kinase signaling (Tomioka et al., 2006; Adachi et al., 2010; Kunitomo et al., 2013). On the other hand, manipulation of the Gq signaling pathway in ASEL has only marginal effect on chemotaxis to NaCl (Adachi et al., 2010). I therefore examined whether the Gq signaling pathway regulates ASEL-dependent chemotaxis. *egl-30(pe914)*, a gain-of-function mutation, is characterized by hyperactive locomotion (Tomioka et al., 2006; Adachi et al., 2010). In the transgenic strain in which *egl-30(pe914)* was expressed in ASEL, the behavioral response was not observed during and after photostimulation of ASEL after cultivation with Na^+ (Fig. 29a&b), suggesting that *egl-30* negatively regulated the response to ASEL stimulation. After Na^+-free cultivation, the transgenic worms showed a small increase of turning behavior during stimulation of ASEL by ChR2 (Fig. 29c&d). These results implied that *egl-30* negatively regulates Na^+ chemotaxis, and possibly the behavioral plasticity in Na^+ chemotaxis.

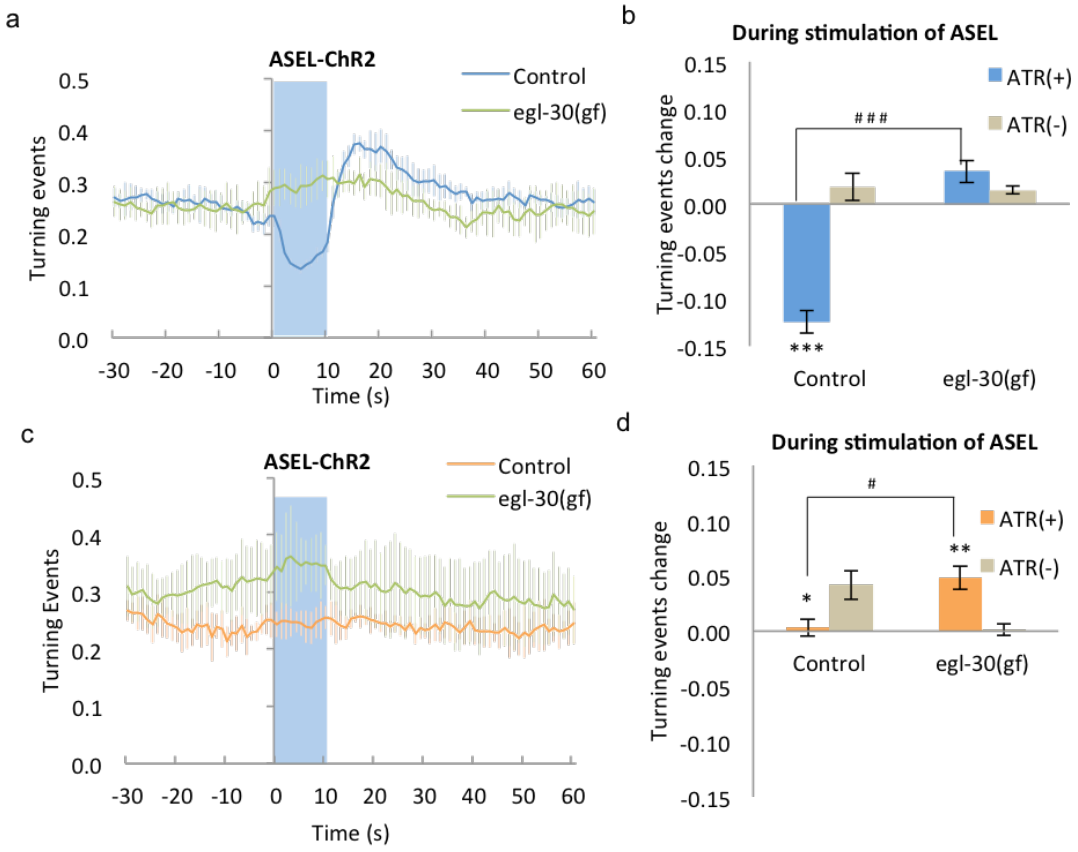

Fig. 29 Behavioral response of *egl-30* trangenic strains to ASEL photoactivation.

a, Behavioral response of a transgenic strain expressing *egl-30* (gf) in ASEL neuron upon ASEL photoactivation at 100 mM Na^+ after cultivation at 50 mM Na^+ (mean ± s.e.m, n ≥ 11). ***b,*** Change of turning event rate in (***a***). Difference between ATR (-) and ATR (+): ***p < 0.001, student *t-test*; difference between strains: ###p < 0.001, student *t-test*. ***c,*** Behavioral response of a transgenic strain expressing *egl-30*(gf) in ASEL neuron upon ASEL photoactivation at 50 mM Na^+ after Na^+-free cultivation (mean ± s.e.m, n ≥ 11). ***d,*** Change of turning event rate in (***c***). Difference between ATR (-) and ATR (+): *p < 0.05, **p < 0.01, student *t-test*; difference between strains: #p < 0.05, student *t-test*.

4. Discussion

4.1 ASEL generates a memory-dependent behavioral plasticity in Na^+ chemotaxis

Unexpectedly, I found that worms generated a memory-dependent behavioral plasticity in Na^+ chemotaxis: when worms were cultivated with Na^+, they migrated to higher Na^+ concentrations (Fig. 1, 22b), whereas when worms were cultivated in the absence of Na^+ and placed onto an Na^+-containing environment, they showed no Na^+ concentration preference (Figs. 1, 23c). Behavioral responses to optogenetic activation of the ASEL neuron roughly recapitulated the chemotaxis responses: worms showed reduction of turning frequency upon activation of ASEL after cultivation with Na^+ (Fig. 2), whereas, they showed no response when they were transferred from Na^+-free cultivation to Na^+-containing conditions (Fig. 23). Calcium imaging combined with optogenetics provided mechanistic insights into Na^+ chemotaxis plasticity: Calcium level of ASEL was increased upon ASEL photostimulation after cultivation with Na^+, however, ASEL showed no calcium response upon photostimulation after worms were cultivated in Na^+-free conditions (Fig. 27). Furthermore, this behavioral plasticity was caused by Na^+, and ASEL could generate Na^+ plasticity by itself.

4.2 Importance for Na^+ plasticity in well-fed conditions

This is the first report to systematically analyze the characteristic of ASEL, which has an important role in Na^+ chemotaxis. The neural mechanism underlying Na^+ plasticity is different from several previously reported behavioral plasticity, such as NaCl chemotaxis plasticity mediated by ASER, in which worms get attracted to NaCl when grown with salt and food (Kunitomo et al., 2013), but avoids NaCl when starved with NaCl (Tomioka et al., 2006; Adachi et al., 2010), odor plasticity, in which when animals are kept with a certain odor without food, they no longer show attraction to that odor (Colbert and Bargmann, 1995), and

concentration-dependent odor chemotaxis, in which odor-sensing neurons switch between high-concentration odor avoidance and low-concentration odor attraction behaviors (Yoshida et al., 2012). All these chemosensory behaviors are mediated by the overlapping neural circuits and our results will extend the platform for further understanding the versatile actions of the small neural circuit of *C. elegans*.

Besides, as one of the mechanisms for learning and memory, changes in neuronal excitability are well documented, for example, long-term changes in piriform cortex (Saar and Barkai, 2009), amygdala (Sehgal et al., 2014) and hippocampus in rodents (Gruart et al., 2012). In these events, voltage-gated and leak cation channels are often involved. Our current findings may lead to recognition of such so far unexplored mechanisms in *C. elegans*. It is necessary to further investigate molecular changes in the ASEL neuron after cultivation without Na^+.

4.3 Comparison with OFF response sensory neurons

The neural circuits functioning downstream of ASEL are in good contrast to that of the well-studied AWC neurons, which mediate chemotaxis to odor (Chalasani et al., 2007, 2010). Both AWC neurons and ASE neurons are glutamatergic neurons (Chalasani et al., 2007; Serrano-Saiz et al., 2013), and, like AWC neurons, I found that glutamatergic neurotransmission from ASEL plays an important role in behavioral response for Na^+ chemotaxis (Fig. 27). AWC neurons are activated by odor removal like ASER (OFF sensory response), while ASEL is activated by the increase in salt concentration (ON sensory response; Chalasani et al., 2007; Suzuki et al., 2008). Furthermore, all these sensory neurons send synaptic outputs to interneurons AIA, AIY, and AIB. However, in contrast to ASEL, AWC releases glutamate to inhibit AIY and AIA and activate AIB to stimulate odor chemotaxis and local search (Chalasani et al., 2007, 2010). Similar to AWC neuron, also an OFF neuron, ASER activates AIB interneurons when the salt concentration is lower than the cultivation concentration to induce worms to migrate to higher salt concentrations in salt chemotaxis (Kunitomo et al., 2013).

ASEL, on the other hand, activates AIA and AIY and inhibits AIB, in a mirror image of AWC. Overall, these interneurons are expected to promote migration to higher Na^+ concentrations given that ASEL shows an ON response after cultivation with Na^+. Our study provides a very interesting cue to understand what differentiates ON and OFF sensory neurons even if they use the same interneurons for behavioral response, and similar neural circuits for regulating chemotaxis. It would be necessary to investigate glutamate receptors used for the synapses between ASEL and these interneurons in Na^+ chemotaxis.

4.4 AIY are more important interneurons than AIA in ASEL-generated Na^+ behavioral response

It should not be ignored that in the neural circuit of ASEL after cultivation with Na^+, AIY and AIA showed similar behavioral responses upon ASEL activation and that AIY-ablation completely eliminated behavioral response when ASEL was stimulated by ChR2 after cultivation with Na^+. AIA-ablation strongly eliminated behavioral response to ASEL's activation when the test Na^+ concentration was different from the cultivation Na^+ concentration (pc ≠ tc), but only diminished it in conditions where Na^+ concentration at pre-assay cultivation was the same as the test condition (pc = tc) (Fig. 6), suggesting that AIY interneuron is more important than AIA for ASEL-driven behavioral responses in Na^+ chemotaxis

4.5 A speculated klinokinesis mechanism based on the neural circuits for the ASEL-generated behavioral response.

Although ASEL, along with ASER, contributes to both klinokinesis and klinotaxis (Iino and Yoshida, 2009), I only examined the effect of ASEL activation on turning behavior, which is the main component of klinokinesis. AIB, AIY and AIA are all important interneurons involved in the klinokinesis mechanism (Iino and Yoshida, 2009; Kunitomo et al., 2013). Activation or ablation of each of these neurons affects reversal/turning behaviors (Gray et al., 2005; Kocabas et al.,

2012; Kunitomo et al., 2013; this study). AIA laser-ablated worms show a severe defect in the klinokinesis mechanism (Iino and Yoshida, 2009), AIB receives synaptic input from AIA, and both interneurons are involved in klinokinesis (Iino and Yoshida, 2009; Kunitomo et al., 2013). AIB sends synaptic outputs to command interneurons AVA, AVB and AVE, which regulate forward/reversal locomotion through synaptic outputs to body wall motor neurons, and also to RIM interneurons, which are important for regulation of reversal (Piggott et al., 2011). AIZ interneurons, which receive inputs from AIY, are essential interneurons for the klinokinesis mechanism (Iino and Yoshida, 2009) and are also connected to the command interneurons, both directly and indirectly. Also, head motor neurons are important for the turning behavior. RIA neurons, which receive synaptic inputs from both AIY and AIZ and are connected to SMD and RMD motor neurons, are also important for the klinokinesis mechanism. Thus, concerted actions of the primary interneurons AIB, AIY and AIA must be effective in regulating klinokinesis mechanism to generate chemotaxis to Na^+ as well as other ions and odor.

4.6 Gq signaling pathway is involved in ASEL-generated Na^+ plasticity.

Our results indicated that the Gq signaling pathway can act in both ASEL and ASER to regulate behavioral plasticity. Upregulation of the Gq signaling pathway in ASER causes worms' attraction to higher NaCl concentrations not only in starved conditions (Adachi et al., 2010) but also in well-fed conditions (Kunitomo et al., 2013), suggesting that the Gq/PKC pathway has a function in driving worms to higher concentrations (Adachi et al., 2010; Kunitomo et al., 2013). On the other hand, the results showed that activation of *egl-30* in ASEL eliminated acceleration of forward movement upon ASEL stimulation after cultivation with Na^+ (Fig. 29), and caused weak turning during ASEL stimulation after Na^+-free cultivation (Fig. 28), suggesting that the Gq signaling pathway may negatively regulate attraction to Na^+ following cultivation at high Na^+ concentrations. In view of the lateralized characteristics of ASE neurons where

ASEL is activated by increase of NaCl concentrations while ASER neuron is activated by decrease of NaCl concentrations, (Suzuki et al., 2008), it is interesting that the Gq signaling pathway modulates worms' attraction to salts in opposite ways in ASEL and ASER neurons. It would be necessary to investigate the involvement of components of the Gq signaling pathway, such as DAG and *ttx-4*/*pkc-1*, in ASEL for Na^+ chemotaxis (Brundage et al., 1996; Sieburth et al., 2007; Adachi et al., 2010; Kunitomo et al., 2013).

4.7 Glutamate is a possible neurotransmitter between ASEL and the first layer interneurons

eat-4, which encodes a vesicular glutamate transporter, is expressed in ASE neurons (Serrano-Saiz et al., 2013), which implies that ASE neurons release glutamate onto downstream interneurons. According to the results in this paper, *eat-4* was involved in ASEL-generated memory-dependent behavioral response in the condition of cultivation with Na^+, implying that after cultivation with Na^+, worms' behavioral response toward higher concentration requires glutamate release from ASEL. Doctoral thesis from Dr. Hirofumi Sato (2016) also showed that neurotransmitter released from ASER requires EAT-4 as a transporter to send signal to interneuron AIB. Thus, whether glutamate is a neurotransmitter between ASEL and the first layer interneurons needs to be further investigated.

4.8 Another possible role for ASEL in Na^+ chemotaxis

Two sets of conditions were investigated in this thesis: cultivation with Na^+, and transfer from cultivation with Na^+-free conditions to Na^+-present test conditions. However, another condition has not been shown in this thesis yet. It is the ASEL's response to stimulation under Na^+-free test conditions after cultivation without Na^+. In this condition, calcium level of ASEL was increased when test concentration was changed from 0 mM to 50 mM (Fig. D1), and the magnitude of the calcium response was about triple of the magnitude of the response to the same test concentration change after cultivation with Na^+, in which case ASEL's

calcium level was just increased by 30 % (Fig. 12a). It suggested a possibility that ASEL may be turned on when worms contact with Na^+ at the first time. It will be necessary to prove this interesting hypothesis.

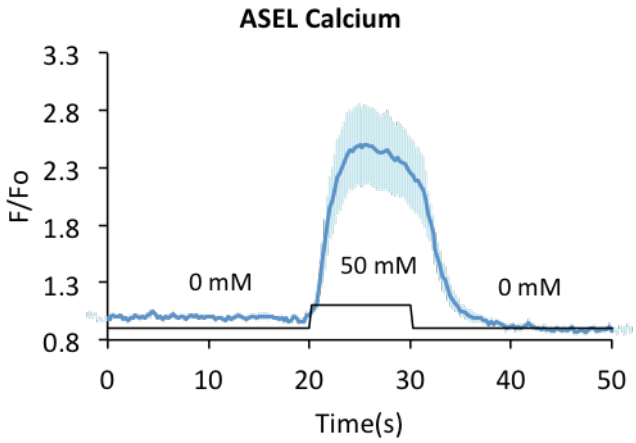

Fig. D1 Calcium response of ASEL to Na^+ concentration changes (from 0 mM to 50 mM) when worms were cultivated without Na^+.

The strain used here is *lite-1 (ce314) X; peIs1095[gcy7p:: ChR 2Y2::venus unc-122p:: mCherry]; Ex[gcy-7p::RGECO; lin-44::gfp]*.

5. Conclusions

In this paper, I found a memory-dependent behavioral plasticity in Na^+ chemotaxis in *C. elegans*, and ASEL could generate this Na^+ plasticity by itself: when worms were cultivated with Na^+, ASEL was activated by photoactivation, as judged by the increase in intracellular Ca^{2+}, and worms showed increased forward movement and positive chemotaxis to Na^+; but when worms were cultivated without Na^+, no change of ASEL calcium level was observed upon ASEL photoactivation, and worms showed no Na^+ concentration preference.

The neural circuit of ASEL-generated behavioral response after cultivation with Na^+ was also dissected in this paper. Under the conditions of cultivation with Na^+, photoactivation of ASEL caused inhibition of its downstream interneuron AIB, which inhibits the turning/reversal behavior, and activation of its downstream interneurons AIY and AIA, which stimulate forward locomotion, overall driving worms towards higher concentrations.

I also found that the Gq signaling pathway and the neurotransmitter glutamate were both involved in the behavioral response generated by ASEL.

Referring to cellular mechanism of behavioral plasticity, I found unexpectedly that Na^+ plasticity generated by ASEL was caused by intrinsic changes of ASEL neuron but not by connectivity changes between ASEL and its interneurons. This may be the first report on the intrinsic excitability for behavioral plasticity in *C. elegans*. As one of the mechanisms for learning and memory, this research proved that it is also conserved in *C. elegans*. Thus, it is necessary to use *C. elegans*, the most understood animal in the world, to further investigate the molecule changes in ASEL after cultivation without Na^+.

6. References

Adachi T, Kunitomo H, Tomioka M, Ohno H, Okochi Y, Mori I, Iino Y. (2010) Reversal of salt preference is directed by the insulin/PI3K and Gq/PKC signaling in *Caenorhabditis elegans*. Genetics186:1309-1319.

Akerboom J, Chen TW, Wardill TJ, Tian L, Marvin JS, Mullu S, Calderón CN, Esposti F, Borghuis BG, Sun XR, Gordus A, Orger MB, Portugues R, Engert F, John J. Macklin JJ, Filosa A, Aggarwal A, Kerr RA, Takagi R, Kracun S, Shigetomi E, Khakh BS, Baier H, Lagnado L, Wang SSH, Bargmann CI, Kimmel BE, Jayaraman V, Svoboda K, Kim DS, Schreiter ER, Looger LL. (2012) Optimization of a GCaMP calcium indicator for neural activity imaging. J Neurosci 32:13819-13840.

Alkon DL. (1984) Calcium-mediated reduction of ionic currents: A biophysical memory trace. Science 226:1037-1045.

Ardiel EL, Rankin CH. (2011) An elegant mind: Learning and memory in *Caenorhabditis elegans*. Learning & Memory 17:191-201.

Bargmann CI, Horvitz RH. (1991) Chemosensory neurons with overlaping functions direct chemotaxis to multiple chemicals in *C. elegans*. Neuron 7, 729-742.

Bargmann CI. (2006) Chemosensation in *C. elegans*. In: WormBook (The *C. elegans* Research Community, ed) doi: 10.1895/wormbook.1.123.1.

Bhatala N, Horvitz HR. (2015) Light and hydrogen peroxide inhibit *C. elegans* feeding through gustatory receptor orthologs and pharyngeal neurons. Neuron 85:804-818.
Brenner S. (1974) The genetics of *Caenorhabditis elegans*. Genetics 77:71–94.

Brundage L, Avery L, Katz A, Kim UJ, Mendel JE, Sternberg PW, Simon MI. (1996) Mutations in a *C. elegans* Gq alpha gene disrupt movement, egg laying, and viability. Neuron 16:999–1009.

Burne T, Scott E, van Swinderen B, Hilliard M, Reinhard J, Claudianos C, Eyles D, McGrath J. (2011) Big ideas for small brains: what can psychiatry learn from worms, flies, bees

and fish? Mol Psychiatry 16:7-16.
Catharine HR. (2002) From gene to identified neuron to behavior in *Caenorhabditis elegans*. Nat Rev Genet 3:622-630.

Chalasani SH, Chronis N, Tsunozaki M, Gray JM, Ramot D, Goodman MB, Bargmann CI. (2007) Dissecting a circuit for olfactory behavior in *Caenorhabditis elegans*. Nature 450:63-70.

Chalasani SH, Kato S, Albrecht DR, Nakagawa T, Abbott LF, Bargmann CI. (2010) Neuropeptide feedback modifies odor-evoked dynamics in *Caenorhabditis elegans* olfactory neurons. Nat Neurosci 13:615–621.

Chandrashekar J, Kuhn C, Oka Y, Yarmolinsky DA, Hummler E, Ryba NJP, Zuker CS. (2010) The cells and peripheral representation of sodium taste in mice. Nature 464:297–301.

Chen Q, Cichon J, Wang W, Qiu L, Lee SR, Campbell NR, DeStefino N, Goard MJ, Fu Z, Yasuda R, Looger LL, Arenkiel BR, Gan WB, Feng G. (2012) Imaging neural activity using Thy1-GCaMP transgenic mice. Neuron 76:297-308.

Chronis N, Zimmer M, Bargmann CI. (2007) Microfluidics for in vivo imaging of neuronal and behavioral activity in *Caenorhabditis elegans*. Nat Methods 4:727-731.

Cleary LJ, Lee WL, Byrne JH. (1998) Cellular correlates of long-term sensitization in *Aplysia*. J Neurosci 18:5988-5998.

Colbert HA, Bargmann CI. (1995) Odorant-specific adaptation pathways generate olfactory plasticity in *C. elegans*. Neuron 14:803-812.

Daoudal G, Debanne D. (2003) Long-term plasticity of intrinsic excitability: Learning rules and mechanisms. Learning&Memory http://www.learnmem.org/cgi/doi/10.1101/lm.64103.

Edwards SL, Charlie NK, Milfort MC, Brown BS, Gravlin CN, Knecht JE, Miller KG. (2008) A novel molecular solution for ultraviolet light detection in *Caenorhabditis elegans*. PLoS Biol 6:1715-1729.

Farley J, Alkon DL. (1985) Cellular mechanisms of learning, memory, and information storage. Annu Rev Psychol 36:419-494.

Fosque BF, Sun Y, Dana H, Yang CT, Ohyama T, Tadross MR, Patel R, Zlatic M, Kim DS, Ahrens MB, Jayaraman V, Looger LL, Schreter ER. (2015) Labeling of active neural circuits in vivo with designed calcium integrators. Science 347:755-760.

Fu Y, Ren M, Feng H, Chen L, Altun ZF, Rubin CS. (2009) Neuronal and intestinal protein kinase D isoforms mediate Na^+ (salt taste)–induced learning. Sci Signal 2:1-13.

Glanzman DL. (2010) Common mechanisms of synaptic plasticity in vertebrates and invertebrates. Curr Biol 20:31-36.

Gray JM, Hill JJ, Bargmann CI. (2005) A circuit for navigation in *Caenorhabditis elegans*. PNAs 102:3184–3191.

Gruart A, Benito E, Delgado-García JM, Barco A. (2012) Enhanced cAMP response element-binding protein activity increases neuronal excitability, hippocampal long-term potentiation, and classical eyeblink conditioning in alert behaving mice.J Neurosci. 32:17431-1741.

Horikawa K, Yamada Y, Matsuda T, Kobayashi K, Hashimoto M, Matsu-ura T, Miyawaki A, Mikoshiba K, Nagai T. (2010) Spontaneous network activity visualized by ultra-sensitive Ca^{2+} indicators, yellow Cameleon-Nano. Nat Methods 7: 729-732.

Hukema RK, Rademakers S, Jansen G (2008) Gustatory plasticity in *C. elegans* involves integration of negative cues and NaCl taste mediated by serotonin, dopamine, and glutamate. Learn Mem 15:829-836.

Husson SJ, Gottschalk A, Leifer AM. (2013) Optogenetic manipulation of neural activity in *C. elegans*: From synapse to circuits and behavior. Biol Cell 105:235-250.

Iino Y, Yoshida K. (2009) Parallel use of two behavioral mechanisms for chemotaxis in *Caenorhabditis elegans.* J Neurosci 29:5370-5380.

Inoue M, Takeuchi A, Horigane S, Ohkura M, Gengyo-Ando K, Fujii H, Kamijo S, Takemoto-Kimura S, Kano M, Nakai J, Kitamura K, Bito H. (2015) Rational design of a high-affinity, fast, red calcium indicator R-CaMP2. Nat Methods 12:64-70.

Jayaraman V, Lauren G. (2007) Evaluating a genetically encoded optical sensor of neural activity using electrophysiology in intact adult fruit flies. Front Neural Circuits 1-3.

Ji G, Feldman ME, Deng KY, Greene KS, Wilson J, Lee JC, Johnston RC, Rishniw M, Tallini Y, Zhang J, Wier WG, Blaustein MP, Xin HB, Nakai J, Kotlikoff MI. (2004) Ca^{2+}-sensing transgenic mice: postsynaptic signaling in smooth muscle. J Biol Chem. 279:21461-21468.

Kandel ER, Tauc L. (1965) Heterosynaptic facilitation in neurons of the abdominal ganglion of *Aplysis depilans*. J Physiol 181:1-27.

Kandel ER. (2001) The molecular biology of memory storage: a dialogue between genes and synapses. Science 294:1030-1038.

Kocabas A, Shen CH, Guo ZV and Ramanathan S. (2012) Controlling interneuron activity in *Caenorhabditis elegans* to evoke chemotactic behavior. Nature 490:273–277.

Kunitomo H, Iino Y. (2008) *Caenorhabditis elegans* DYF-11, an orthologue of mammalian Traf3ip1/MIP-T3, is required for sensory cilia formation. Genes Cells 13:13-25.

Kunitomo H, Sato H, Iwata R, Satoh Y, Ohno H, Yamada K, Iino Y. (2013) Concentration memory-dependent synaptic plasticity of a taste circuit regulates salt concentration chemotaxis in *Caenorhabditis elegans*. Nat Commun 4:1-11.

Lackner M, Nurrish S, Kaplan J. (1999) Facilitation of synaptic transmission by EGL-30 Gq alpha and EGL-8 PLC beta: DAG binding to UNC-13 is required to stimulate acetylcholine release. Neuron 24:335–346.

Larsch J, Flavell SW, Liu Q, Gordus A, Albrecht DR, Bargmann CI. (2015) A circuit for gradient climbing in *C. elegans* chemotaxis. Cell Rep 12:1748-1760.

Lee D, Jung S, Ryu J, Ahnn J, Ha I. (2008) Human vesicular glutamate transporters functionally complement EAT-4 in *C. elegans*. Mol Cells 25:50-54.

Lee RYN, Sawin ER, Chalfie M, Horvitz HR, Avery L. (1999) EAT-4, a homolog of a mammalian sodium-dependent inorganic phosphate cotransporter, is necessary for glutamatergic neurotransmission in *Caenorhabditis elegans*. J Neurosci 19:159-167.

Leinwand SG, Chalasani SH. (2013) Neuropeptide signaling remodels chemosensory circuit composition in *Caenorhabditis elegans*. Nat neurosci 16:1461-1467.

Li Z, Liu J, Zheng M, Xu XZS. (2014) Encoding of both analog- and digital-like behavioral outputs by one *C. elegans* interneuron. Cell 159:751–765.

Liu J, Ward A, Gao J, Dong Y, Nishio N, Inada H, Kang L, Yu Y, Ma D, Xu T, Mori I, Xie Z, Xu SXZ. (2010) *C. elegans* phototransduction requires a G protein–dependent cGMP pathway and a taste receptor homolog. Nat Neurosci 13:715-722.

Matsuki M, Kunitomo H, Iino Y. (2006) Goα regulates olfactory adaptation by antagonizing Gqα-DAG signaling in *Caenorhabditis elegans*. Proc. Natl Acad. Sci. USA 103:1112–1117.

Miller AC, Thiele TR, Faumont S, Moravec ML, Lockery SR. (2005) Step-Response Analysis of Chemotaxis in *Caenorhabditis elegans*. J Neurosci 25:3369 –3378.

Muto A, Ohkura M, Kotani T, Higashijima S, Nakai J, Kawakami K. (2011) Genetic visualization with an improved GCaMP calcium indicator reveals spatiotemporal activation of the spinal motor neurons in zebrafish. PNAs 108:5425-5430.

Nagai T, Yamada S, Tominaga T, Ichikawa M, Miyawaki A. (2004) Expanded dynamic range of fluorescent indicators for Ca^{2+} by circularly permuted yellow fluorescent proteins. PNAs 101:10554-10559.

Nakai J, Ohkura M, Imoto K. (2001) A high signal-to-noise Ca^{2+} probe composed of a single green fluorescent protein. Nat Biotech 19:137-141.

Oda S, Tomioka M, Iino Y. (2011) Neuronal plasticity regulated by the insulin-like signaling pathway underlies salt chemotaxis learning in *Caenorhabditis elegans*. J neurophysiol 106:301-308.

Ohkura M, Sasaki T, Kobayashi C, Ikegaya Y, Nakai J. (2012) An improved genetically encoded red fluorescent Ca^{2+} indicator for detecting optically evoked action potentials. PLoS ONE 7:e39933.

Ohkura M, Sasaki T, Sadakari J, Gengyo-Ando K, Kagawa-Nagamura Y, Kobayashi C, Ikegaya Y, Nakai J. (2012). Genetically encoded green fluorescent Ca^{2+} indicators with improved detectability for neuronal Ca^{2+} signals. PLoS ONE DOI: 10.1371/journal.pone.0051286.

Ortiz CO, Faumont S, Takayama J, Ahmed HK, Goldsmith AD, Pocock R, McCormick KE, Kunimoto H, Iino Y, Lockery S, Hobert O. (2009) Lateralized gustatory behavior of *C. elegans* is controlled by specific receptor-type guanylyl cyclases. Curr Biol 8:996-1004.

Perkins LA, Hedgecock EM, Thomson JN, Culotti JG. (1986). Mutant sensory cilia in the nematode *Caenorhabditis elegans*. Dev. Biol. 117: 456–487.

Pierce-Shimomura JT, Morse TM, Lockery SR (1999) The fundamental role of pirouettes in *Caenorhabditis elegans* chemotaxis. J Neurosci 19:9557–9569.

Piggott BJ, Liu J, Feng Z, Wescott SA, Xu XZS. (2011) The neural circuits and synaptic mechanisms underlying motor initiation in *C. elegans* Cell 147:922-933.

Rand JB, Duerr JS, Frisby DL. (2000) Neurogenetics of vesicular transporters in *C. elegans*. FASEB J 14:2414-2422.

Saar D, Barkai E. (2009) Long-lasting maintenance of learning-induced enhanced neuronal excitability: mechanisms and functional significance. Mol Neurobiol 39:171–177.

Saeki S, Yamamoto M, Iino Y. (2001) Plasticity of chemotaxis revealed by paired presentation of a chemoattractant and starvation in the nematode *Caenorhabditis elegans*. J Exp Biol 204:1757–1764.

Sasakura H, Mori I. (2012) Behavioral plasticity, learning, and memory in *C. elegans*. Curr Opin Neurobiol 23:1-8.

Satoh Y, Sato H, Kunitomo H, Fei X, Hashimoto K, Iino Y. (2014) Regulation of experience-dependent bidirectional chemotaxis by a neural circuit switch in *Caenorhabditis elegans*. J Neurosci 34:15631-15637.

Sehgal M, Ehlers VL, Moyer JR. (2014) Learning enhances intrinsic excitability in a subset of lateral amygdala neurons. Learn Mem 21:161–170.

Serrano-Saiz E, Poole RJ, Felton T, Zhang F, Cruz ED, Hobert O. (2013) Modular control of glutamatergic neuronal identity in *C. elegans* by distinct homeodomain proteins. Cell 155:659-673.

Sieburth D, Madison J, Kaplan J. (2007) PKC-1 regulates secretion of neuropeptides. Nat Neurosci 10: 49-57.

Stein GM, Murphy CT. (2014) *C. elegans* positive olfactory associate memory is a molecularly conserved behavioral paradigm. Neurobiol Learn Mem http://dx.doi.org/10.1016/j.nlm.2014.07.011

Suzuki H, Thiele TR, Faumont S, Ezcurra M, Lockery SR, Schafer WR. (2008) Functional asymmetry in *Caenorhabditis elegans* taste neurons and its computational role in chemotaxis. Nature 454:114-117.

Tallini YN, Ohkura M, Choi BR, Ji G, Imoto K, Doran R, Lee J, Plan P, Wilson J, Xin HB, Sanbe A, Gulick J, Mathai J, Robbins J, Salama G, Nakai J, Kotlikoff MI. (2006) Imaging cellular signals in the heart in vivo: Cardiac expression of the high-signal Ca^{2+} indicator GCaMP2. PNAS 103:4753-4758.

Tian L, Hires SA, Mao T, Huber D, Chiappe ME, Chalasani SH, Petreanu L, Akerboom J, McKinney SA, Schreiter ER, Bargmann CI, Jayaraman V, Svoboda K, Looger LL. (2009) Imaging neural activity in worms, flies and mice with improved GCaMP calcium indicators. Nat. Methods 6:875-881.

Tomioka M, Adachi T, Suzuki H, Kunitomo H, Schafer WR, Iino Y. (2006) The insulin/PI 3-kinase pathway regulates salt chemotaxis learning in *Caenorhabditis elegans*. Neuron 51:613-625.

Walker AS, Burrone J, Meyer MP. (2013) Functional imaging in the zebrafish retinotectal system using RGECO. Front Neural Circuits 7:1-10.

Wang Q, Shui B, Kotlikoff M, Sondermann H. (2008) structural basis for calcium sensing by GCaMP2. Structure. 16:1817-1827.

White JG, Southgate E, Thomson JN, Brenner S. (1986) The structure of the nervous system of the nematode *Caenorhabditis elegans*. Philos Trans R Soc Lond B Biol Sci 314:1–340.

Wu J, Liu L, Matsuda T, Zhao Y, Rebane A, Drobizhev M, Chang YF, Araki S, Arai Y, March K, Hughes TE, Sagou K, Miyata T, Nagai T, Li WH, Campbell RE. (2013) Improved orange and red Ca^{2+} indicators and photophysical considerations for optogenetic applications. ACS Chem. Neurosci 4:963-972.

Yizhar O, Fenno LE, Davidson T, Mogri M, Deisseroth K. Optogenetics in neural systems. Neuron 71:9-18.

Yoshida K, Hirotsu T, Tagawa T, Oda S, Wakabayashi T, Iino Y, Ishihara T. (2012) Odour concentration-dependent olfactory preference change in *C. elegans*. Nat Commun 3:739. doi: 10.1038/ncomms1750.

Yoshihara M. (2012) Simultaneous recording of calcium signals from identified neurons and feeding behavior of Drosophila melanogaster. J Vis Exp 62: 3625.

Yoshina S, Sakaki K, Yonezumi-Hayashi A, Gengyo-Ando K, Inoue H, Iino Y, Mitani S. (2012) Identification of a novel ADAMTS9/GON-1 function for protein transport from the ER to the Golgi. Mol Biol Cell 9:1728-1741.

Zhang F, Aravanis AM, Adamantidis A, Lecea Ld, Deisseroth K. (2007) Circuit-breakers: optical technologies for probing neural signals and systems. Nat Neurosci 8:577-581.

Zhang F, Wang LP, Brauner M, Liewald JF, Kay K, Watzke N, Wood PG, Bamberg E, Nagel G, Gottschalk A, Deisseroth K. (2007) Nature 446:633-641.

Zhang YV, Ni J, Montell C. (2013) The molecular basis for attractive salt-taste coding in *Drosophila*. Science 340:1334-1338.

Zhao Y, Araki S, Wu J, Teramoto T, Chang YF, Nakano M, Abdelfattah AS, Fujiwara M, Ishihara T, Nagai T, Campbell RE. (2011) An expanded palette of genetically encoded Ca^{2+} indicators. Science 333:1888–1891.

7. Acknowledgements

I would like to thank Dr. Takeshi Ishihara for the plasmid *pDEST-RGECO*, Drs. Keiko Gengyo-Ando, Junichi Nakai and Haruhiko Bito for the plasmid *pDEST-RCaMP2*, Drs. Oliver Horbet and Chris Ortiz for the ASEL-ablated strain (OH9019), Dr. Tokumitsu Wakabayashi for AWC-ablated strain.

I could have never been able to accomplish this work, nor would I have even made it to graduate to thank my supervisor and mentor, Prof. Yuichi Iino, for instructing me on valuable skills to develop logical thinking, deep perspective, and how to write manuscripts, and for the amazingly dependable source of support and patience until graduation. Within the nurturing environment of his lab, I felt encouraged to be myself to follow my own path. Under the financial support, I enjoyed in the scientific atmosphere and conversations with scientists with different cultures in Japanese and international conferences. Yet, he also has a wonderful sense of humor, I'm truly lucky to have had him as my supervisor.

For the past 5 years, the Iino lab has been my family, and I am grateful to lab members for their contributions to my scientific development, as well as for friendship and personal support. Great thankful to my group members Dr. Hirofumi Sato and Dr. Yohsuke Satoh, I'd say I could not have finished the optogenetic-calcium imaging research without their helps, they have always been there when I need help or advices. I would like to thank Dr. Masahiro Tomioka and Dr. Hirofumi Kunitomo for technical advices on chemotaxis assay and behavioral assay, and for advices in the manuscript. I also would like to thank Dr. Yu Toyoshima for the advices in the experiments of ChR2-RCaMP2 system. I am particularly grateful to the technician Ms. Manami Kanamori for the microinjections.

Giving my thanks to the lab manager Yukako Iwahara for procedures during the five years. Thank to my tutors, Dr. Kazushi Yoshida, Dr. Hirofumi Sato, and especially Dr. Naoko Sakai for the help in daily life during the five years in Japan. Thank you all lab members for all the cherished memories during the five years, I

have enjoyed your jokes and friendship. I also would like to thank to the members of International Liason Office and Affairs Office of Department of Biological Science for procedures at work and for daily like to help me go through the life in Japan comfortably as an international student.

Lastly, I am thankful for my family. My Mom has always been my hero, my father's words always strengthen me up, and the unwavering love and support from them have allowed me to accomplish so much. My little brother is always at hometown, which has allowed me go anywhere without worrying about the family. I am also grateful to my mother-in-low and father-in-law for selflessly helping take care of my daughter to my graduation and bringing up a good man as my husband. Thanks to all my family members and friends for all the mental supports during the long periods of student lifetime.